

HTLV-1 bZIP Factor Suppresses Apoptosis by Attenuating the Function of FoxO3a and Altering Its Localization

Azusa Tanaka-Nakanishi, Jun-ichirou Yasunaga, Ken Takai, and Masao Matsuoka

Abstract

As the infectious agent causing human adult T-cell leukemia (ATL), the human T-cell leukemia virus type 1 (HTLV-1) virus spreads *in vivo* primarily by cell-to-cell transmission. However, the factors that determine its transmission efficiency are not fully understood. The viral genome encodes the HTLV-1 bZIP factor (HBZ), which is expressed in all ATL cases and is known to promote T-cell proliferation. In this study, we investigated the hypothesis that HBZ also influences the survival of T cells. Through analyzing the transcriptional profile of HBZ-expressing cells, we learned that HBZ suppressed transcription of the proapoptotic gene *Bim* (*Bcl211*) and that HBZ-expressing cells were resistant to activation-induced apoptosis. Mechanistic investigations into how HBZ suppresses *Bim* expression revealed that HBZ perturbs the localization and function of FoxO3a, a critical transcriptional activator of the genes encoding *Bim* and also *FasL*. By interacting with FoxO3a, HBZ not only attenuated DNA binding by FoxO3a but also sequestered the inactive form of FoxO3a in the nucleus. In a similar manner, HBZ also inhibited *FasL* transcription induced by T-cell activation. Further study of ATL cells identified other *Bim* perturbations by HBZ, including at the level of epigenetic alteration, histone modification in the promoter region of the *Bim* gene. Collectively, our results indicated that HBZ impairs transcription of the *Bim* and *FasL* genes by disrupting FoxO3a function, broadening understanding of how HBZ acts to promote proliferation of HTLV-1-infected T cells by blocking their apoptosis. *Cancer Res*; 74(1); 188–200. ©2013 AACR.

Introduction

Human T-cell leukemia virus type 1 (HTLV-1) is estimated to infect 10 to 20 million people in the world (1). This virus causes not only a neoplastic disease of CD4⁺ T cells, adult T-cell leukemia (ATL), but also chronic inflammatory diseases of the central nervous system, lung, or skin (2). HTLV-1 can be transmitted efficiently in a cell-to-cell fashion (3, 4), whereas free virus shows poor infectivity (5, 6), and virions are not detected in infected individuals. To increase the number of infected cells and facilitate transmission, HTLV-1 increases its copy number primarily by triggering the proliferation of infected cells, replicating within the host genome instead of undergoing viral replication (7, 8). Thus, HTLV-1 promotes proliferation and suppresses apoptosis of infected cells via complex interactions of viral proteins with host factors.

Among the viral genes encoded in HTLV-1, the *tax* gene has been extensively studied. *Tax* can activate various signal pathways like NF- κ B, AP-1, and SRF (9). However, *Tax* expression is

frequently undetectable in ATL cases. Importantly, the non-sense mutations in the *tax* gene are often observed in not only ATL cases but also infected cells of asymptomatic HTLV-1 carriers (10). These findings suggest that other mechanisms suppress the apoptosis of HTLV-1-infected cells in the absence of *Tax* expression (2). We have reported that the *HTLV-1 bZIP factor* (*HBZ*) gene is expressed in all ATL cases (11). Furthermore, HBZ promotes the proliferation of T cells and induces development of T-cell lymphomas and inflammatory diseases in transgenic mice (12). Therefore, we speculated that HBZ might also influence apoptosis.

There are two major pathways for apoptosis: the extrinsic and intrinsic apoptotic pathways, which are mediated by *Fas* and *Bim*, respectively (13). ATL cells are known to express high levels of *Fas* antigen, and are susceptible to *Fas*-mediated signaling (14). However, *FasL* expression is suppressed in ATL cells by silencing of the *early growth response 3* (*EGR3*) gene transcription, a phenomenon that enables ATL cells to escape activation-induced cell death (15). In addition, *Tax* increases expression of *c-FLIP*, which confers resistance to *Fas*-mediated apoptosis (16, 17). Furthermore, activation of NF- κ B by *Tax* also enables HTLV-1-infected cells to be resistant to apoptosis (18). To date, the effects of HTLV-1 infection on *Bim*-mediated apoptosis remain unknown.

In this study, we analyzed transcriptional changes induced by HBZ expression in T cells, and found that transcription of a proapoptotic gene, *Bim*, was hindered by HBZ. This suppression led to decreased activation-induced cell death. We found that HBZ suppressed *Bim* transcription by targeting FoxO3a, a critical transcription factor for the *Bim* and *FasL* gene. In some

Authors' Affiliation: Laboratory of Virus Control, Institute for Virus Research, Kyoto University, Sakyo-ku, Kyoto, Japan

Note: Supplementary data for this article are available at Cancer Research Online (<http://cancerres.aacrjournals.org/>).

Corresponding Author: M. Matsuoka, Institute for Virus Research, Kyoto University, 53 Shogoin Kawahara-cho, Sakyo-ku, Kyoto 606-8507, Japan. Phone: 81-757-514-048; Fax: 81-757-514-049; E-mail: mmatsuok@virus.kyoto-u.ac.jp

doi: 10.1158/0008-5472.CAN-13-0436

©2013 American Association for Cancer Research.

ATL cell lines and ATL cases, the *Bim* gene transcription was also silenced by epigenetic mechanisms, but this phenomenon seemed to be secondary to HBZ-mediated suppression of transcription. Thus, it is suggested that HBZ suppresses both intrinsic and extrinsic apoptotic pathways and contributes to the proliferation of ATL cells.

Materials and Methods

Cell lines and clinical samples

HTLV-1 immortalized cell lines (MT-4), ATL cell lines (ED, TL-Om1, and MT-1), T-cell lines not infected with HTLV-1 (Jurkat, SupT1, and CCRF-CEM) were cultured in RPMI 1640 medium supplemented with 10% FBS and antibiotics at 37°C under a 5% CO₂ atmosphere. Jurkat cells stably expressing spliced form of HBZ (sHBZ), Jurkat-HBZ, were maintained as described previously (19). To construct CCRF-CEM cells stably expressing HBZ, CEM-HBZ, the coding sequence of HBZ was subcloned into pME18Sneo vector and then the expression vector or its empty vector were transfected into CCRF-CEM cells by using Neon (Invitrogen) according to the manufacturer's instructions. Stable transfectants were selected in G418 (1 mg/mL). 293T cells were cultured in Dulbecco's Modified Eagle Medium supplemented with 10% FBS and antibiotics and when 293FT cells were cultured, 500 µg/mL G418 was added. Fas-blocking antibody was purchased from Alexis.

This study was conducted according to the principles expressed in the Declaration of Helsinki. The study was approved by the Institutional Review Board of Kyoto University (G204). All patients provided written informed consent for the collection of samples and subsequent analysis.

Plasmid constructs

Wild-type form of FoxO3a was generated by PCR amplification using Jurkat cDNA library and constitutively active form of FoxO3a (FoxO3aAAA) was also generated by PCR amplification with mutated primers (20). These PCR fragments were then subcloned into pCMV-Tag2B vector and pIRES-hrGFP-1a (Stratagene). The vectors encoding the myc-His-tagged form of HBZ and its mutants used in this study have been described previously (19, 21). We modified pLKO.1-EGFP vector for delivery of anti-FoxO3 short hairpin RNAs (shRNA) to Jurkat, Jurkat-control, and Jurkat-HBZ. shRNA sequence used was 5'-GCACAACCTGTCTGCATAG-3'. The 6xDBE-Luc construct that contains six FOXO-binding sites known as DAF-16 binding elements (DBE) was kindly provided by Dr. Furuyama (Kagawa Prefectural University of Health Sciences, Kagawa, Japan) and the backbone of this vector was pGL3-basic (Promega; ref. 22).

Luciferase assay

Jurkat cells were transfected with 0.2 µg/well of luciferase reporter plasmid, 1 ng/well of *Renilla* luciferase control vector (phRL-TK), 0.2 µg/well of FoxO3aAAA expression plasmid or its empty vector, and 0.6 µg/well of HBZ expression plasmid or its empty vector with caspase inhibitor Z-VAD-FMK (MBL). Plasmids were transfected using Neon (Invitrogen) according to the manufacturer's instructions. After 24 hours, cells were collected and luciferase activities were measured using the

Dual-Luciferase Reporter Assay (Promega). Relative luciferase activity was calculated as the ratio of firefly to *Renilla* luciferase activity. Three independent experiments, each with triplicate transfections, were performed and typical results are shown.

Microarray analysis

Jurkat-control and Jurkat-HBZ were stimulated with phorbol myristate acetate (PMA; 50 ng/mL) and ionomycin (Io; 1 µg/mL) for 9 hours. After the stimulation, cells were collected and total RNA was isolated using TRIzol Reagent (Invitrogen) according to the manufacturer's instructions. We then digested DNA using deoxyribonuclease I (Invitrogen) and cleaned up RNA using RNeasy Mini Kit (Qiagen) according to the manufacturer's instructions. We then synthesized cDNA and performed microarray processing according to the GeneChip Expression Analysis Technical Manual (Affymetrix). All data were analyzed by using GeneSpring GX (Agilent Technologies). The microarray data related to this article have been submitted to the Gene Expression Omnibus under the accession number GSE48029.

Immunofluorescence analysis

293FT cells were transfected with expression vectors using Lipofectamine LTX (Invitrogen) or TransIT (TaKaRa). Twenty-four hours after transfection, cells were reseeded on the poly-L-lysine-coated glass (Matsunami Glass Ind., Ltd.) or poly-D-lysine (Sigma)-coated glass. Twenty-four hours after the reseeding, cells were fixed with 4% paraformaldehyde for 15 minutes and permeabilized with 0.2% Triton X-100 for 15 minutes, and blocked by incubation in 5% BSA/PBS for 30 minutes. For immunostaining, the cells were incubated with anti-Foxo3a, anti-p-Foxo3a (Cell Signaling Technology), Cy3-conjugated anti-c-Myc (Sigma) or biotinylated anti-FLAG (Sigma) antibodies for 1 hour or in case of observation of endogenous expression, cells were incubated overnight at 4°C. Primary antibodies were visualized by incubating the cells with AlexaFluor 488-conjugated goat anti-rabbit immunoglobulin G (IgG) antibody (Invitrogen) or AlexaFluor 488-conjugated streptavidin (Invitrogen). Nuclei were stained and mounted with ProLong Gold antifade reagent with 4',6-diamidino-2-phenylindole (DAPI; Invitrogen). To concentrate nonadherent cells onto a microscope slide, CytoFuge (StatSpin) was used. Fixation and blocking were performed as described earlier.

Assessment of apoptosis

Apoptotic cells were routinely identified by Annexin V-APC (eBioscience) or phycoerythrin (PE) or fluorescein isothiocyanate (FITC; BioVision) -staining according to the manufacturer's instructions and analyzed with a flow cytometer (BD FACSCanto II; BD Biosciences). Data files were analyzed by using FlowJo software (TreeStar).

Real-time PCR

Total RNA was isolated for the analysis using TRIzol reagent. RNA was treated with DNase I to eliminate the genomic DNA. Reverse transcription was performed using random primer and SuperScript III Reverse Transcriptase (Invitrogen). CD25⁻ CD4⁺ cells from healthy donor were obtained by using human

CD4 T Lymphocyte Enrichment kit (BD Pharmingen). Then, cells were stimulated with PMA/Io for 9 hours, RNA was isolated, and reverse transcription was performed as described earlier. cDNA products were analyzed by real-time PCR using the Taqman Universal PCR Master Mix (PE Applied Biosystems) or FastStart Universal SYBR Green Master (Roche) and Applied Biosystems StepOnePlus Real-Time PCR System according to the manufacturer's instructions. Specific primers and Taqman probes for the *Bim* gene, *FasL* gene, and *GAPDH* internal control gene were purchased from Applied Biosystems. Primer sequences for the *HBZ* gene and *GAPDH* gene used for the evaluation of the knockdown efficiency in MT-1 cells have been described previously (11, 23). Primer sequences for the *HBZ* gene used for another experiment to evaluate the *HBZ* expression in Jurkat-HBZ, MT-1, TL-Om1, and ED cells were 5'-ATGGCGCCTCAGGGCTGTT-3' and 5'-GCGGC-TTTCCTCTTAAGG-3'. Primer sequences for the *FoxO3a* gene used were 5'-ACAAACGGCTCACTCTGTCCAG-3' and 5'-AGCTCTTGCCAGTTCCCTCATTCTG-3'. All amplifications were conducted in triplicates. The relative quantification was calculated according to the method described in Applied Biosystems ABI prism 7700 SDS User Bulletin #2.

Chromatin immunoprecipitation analysis

Chromatin immunoprecipitation (ChIP) assay was performed according to the protocol recommended by Millipore. Cells were fixed with 1% formaldehyde for 10 minutes at room temperature, washed twice with ice-cold PBS, treated with SDS-lysis buffer (1% SDS, 50 mmol/L EDTA, and 200 mmol/L Tris-HCl) for 10 minutes on ice and then sonicated. Thereafter, the DNA/protein complexes were immunoprecipitated with antibodies specific for acetylated-Histone H3, acetylated-Histone H4, dimethylated-Histone H3 (Lys4), RNA polymerase II clone CTD4H8 (Millipore), trimethylated-Histone H3 (Lys27), anti-trimethyl-Histone H3 (Lys9) antibodies (Cell Signaling Technology), or normal rabbit IgG (Santa Cruz Biotechnology) overnight at 4°C. Immune complexes were collected with salmon sperm DNA-protein A and G Sepharose slurry, washed, and eluted with freshly prepared elution buffer (1% SDS, 100 mmol/L NaHCO₃). Protein-DNA complexes were de-cross-linked at 65°C for 4 hours. DNA was purified and subjected to real-time PCR for quantification of the target fragments. Sequences for the primer set are described previously (24, 25). For the evaluation of binding of FoxO3a to the FOXO-binding sites, 293T cells were transfected with 5 µg of 6xDBE-Luc construct, 5 µg of FoxO3aAAA expression plasmid together with or without 5 µg of HBZ plasmid using TransIT in 10-cm dishes. Anti-FLAG (Sigma) antibody was used for the immunoprecipitation. Primers used were 5'-AGTGCAGGTGCCA-GAACATT-3' and 5'-GCCTTATGCAGTTGCTCTCC-3', which were constructed inside of the pGL3-basic vector. For the evaluation of the DNA-binding capacity of FoxO3a with or without HBZ, expression vectors for the HA-tagged FoxO3a and Flag-tagged HBZ were transiently cotransfected into 293T cells using the TransIT reagent. Twenty-four hours after the transfection, cells were collected and chromatin immunoprecipitation assay was performed as described earlier. For the immunoprecipitation, anti-HA (Sigma) antibody was used.

Primers used for *Bim* gene promoter were 5'-CCACCACTT-GATTCTTGCAG-3' and 5'-TCCAGCGCTAGTCTTCCTTC-3', which were constructed to contain the FOXO-binding sequence located in intron1. Primers used for *FasL* gene promoter were 5'-ACGATAGCACCCTGCACTCC-3' and 5'-GGCTGCAAACCACTGGAAC-3', which were also constructed to contain the three FOXO-binding sequences.

Individual PCRs were carried out in triplicate to control for PCR variation and mean C_t values were collected. Fold difference of the antibody-bound fraction (IP) versus a fixed amount of input (In) was calculated as

$$IP/In = 2^{-\Delta\Delta C_t} = 2^{-(C_t(IP) - C_t(In))}$$

Then, the fold difference value for a target antibody (t) was subtracted by the nonspecific value derived from mouse or rabbit IgG (t₀):

$$(IP/In)^t - (IP/In)^{t_0}$$

Bisulfite genomic sequencing

Sodium bisulfite treatment of genomic DNA was performed as described previously (26). DNA regions were amplified using bisulfite-treated genomic DNA by nested PCR. To amplify promoter region (promoter 1) of *Bim*, primers used in the first PCR were 5'-TTTAGAGGGAGGAGAGTTTAAAG-3' and 5'-CCCTACAACCCAACTCTAACTA-3'. Primers for the second PCR were 5'-AGGGTATAGTGAGAGCGTAGG-3' and 5'-CAACTCTAACTAACGACCCC-3'. For promoter, two primers used in the first PCR were 5'-GTGTGATTGTTTTTGAGGG-3' and 5'-AAAATACCCCAAACAAAATAC-3'. Primers for the second PCR were 5'-GCGGATTTAGTTGTAGATTTTG-3' and 5'-ACTCTTTACCCAAAACAACTTC-3'. PCR products were purified, cloned into pGEM-T Easy vector (Promega), and sequenced using the ABI PRISM 3130 Genetic Analyzer. For CpG methylation analysis, Web-based bisulfite sequencing analysis tool called QUMA (quantification tool for methylation analysis) was used (27).

Coimmunoprecipitation assay, analysis of the p-FoxO3a localization, and immunoblotting

Expression vectors for the relevant genes were transiently cotransfected into 293T cells using the TransIT reagent. Forty-eight hours later, cells were collected and coimmunoprecipitation assays were performed as described previously (28). For the analysis of the p-FoxO3a localization, nuclear and cytoplasmic proteins were extracted using Nuclear Complex Co-IP Kit (Active Motif). The proteins were subjected to SDS-PAGE analysis followed by immunoblotting with various antibodies. Antibodies used were anti-p-FoxO3a, anti-α-tubulin (Sigma), anti-FLAG, anti-HA (Sigma), and anti-His (Marine Biological Laboratory).

Lentiviral vector construction and transfection of the recombinant lentivirus

Lentiviral vector expressing shRNA against HBZ was constructed and recombinant lentivirus was infected as described previously (11). When more than 90% of cells expressed

enhanced green fluorescent protein (EGFP), the *HBZ* and *Bim* gene expressions were analyzed by real-time PCR.

Results

The *Bim* gene transcription is suppressed in HBZ-expressing Jurkat and CCRF-CEM cells

To determine the effects of HBZ on gene expression, we first performed microarray analysis. Jurkat cells with or without expression of spliced form of HBZ (Jurkat-HBZ and Jurkat-control, respectively) were stimulated with PMA and Io for 9 hours. Gene expression profiles were then analyzed by DNA microarray. Table 1 shows the apoptosis-associated genes that were downregulated or upregulated in stimulated Jurkat-HBZ cells. Transcription of the *Bim* gene was prominently downregulated in HBZ-expressing Jurkat cells. To confirm the effect of HBZ on the *Bim* gene expression, we evaluated *Bim* mRNA levels in Jurkat-control and Jurkat-HBZ cells with or without PMA/Io stimulation using real-time PCR. As reported in the previous studies showing that treatment by PMA/Io or other stimulators induced *Bim* expression (29, 30), the *Bim* mRNA level of stimulated Jurkat-control cells was three-times higher than that of unstimulated cells, but that of Jurkat-HBZ cells did not change after stimulation (Fig. 1A). Similarly, increased *Bim* transcription by stimulation was also inhibited by HBZ in CCRF-CEM cells (Fig. 1A).

HBZ inhibits apoptosis

It has been reported that *Bim* plays an important role in activation-induced cell death and T-cell homeostasis (31).

Because the earlier data demonstrated that HBZ inhibits stimulation-induced *Bim* expression, we next investigated whether HBZ inhibits apoptosis in response to PMA/Io stimulation. To test this, Jurkat-control and Jurkat-HBZ were each incubated with or without PMA/Io for 9 hours, and then apoptosis was measured using Annexin V. The percentages of apoptotic cells in Jurkat-control and Jurkat-HBZ were 40.2% and 15% respectively, indicating that HBZ suppressed activation-induced apoptosis (Fig. 1B). We also treated cells with doxorubicin and found that HBZ slightly inhibited doxorubicin-induced apoptosis (Supplementary Fig. S1). Fas-mediated apoptotic pathway might be involved in antiapoptotic effect by HBZ. To assess the effect of Fas-mediated signaling on the activation-induced apoptosis, cells were also treated with or without Fas-blocking antibody (0.5 $\mu\text{g}/\text{mL}$) 30 minutes before the PMA/Io stimulation. The percentage of apoptotic cells without Fas-blocking antibody in Jurkat-control and Jurkat-HBZ were 36.9% and 22.4%, respectively. When cells were treated with Fas-blocking antibody, the percentage of apoptotic cells reduced and those were 24% and 13.2% in Jurkat-control and Jurkat-HBZ, respectively (Fig. 1C). Thus, Fas-blocking antibody partially inhibited apoptosis in Jurkat-HBZ, which indicates that Fas-mediated signals are also implicated in activation-induced cell death. Indeed, we found that the transcription level of *FasL* was suppressed in stimulated Jurkat-HBZ and CEM-HBZ cells compared with Jurkat-control and CEM-control cells (Fig. 1D), suggesting that downregulation of *FasL* by HBZ was also associated with inhibition of apoptosis.

Table 1. Apoptosis-associated genes that are upregulated or downregulated by HBZ

Gene	Fold change	Gene ontology
API5	2.18	Antiapoptosis
BCL2L11 (<i>Bim</i>)	-9.93	Induction of apoptosis
CARD11	2.87	Regulation of apoptosis
CASP1	2.97	Apoptosis
CD28	4.60	Positive regulation of antiapoptosis
COP1	9.41	Regulation of apoptosis
DEDD2	2.01	Induction of apoptosis via death domain receptors
DYRK2	2.16	Induction of apoptosis
GZMB	-5.90	Apoptosis
HIPK2	2.19	Induction of apoptosis by intracellular signals
NLRP1	3.08	Induction of apoptosis
PI3KR2	-2.68	Negative regulation of antiapoptosis
PLEKHF1	2.99	Induction of apoptosis
PRDX2	-2.10	Antiapoptosis
PRF1	3.95	Virus-infected cell apoptosis
RFFL	2.20	Apoptosis
SPHK1	-4.26	Antiapoptosis
TNFRSF9	-2.61	Induction of apoptosis
TP53INP1	2.32	Apoptosis
VEGFA	-6.96	Negative regulation of apoptosis

NOTE: The table shows a list of apoptosis-associated genes that were downregulated or upregulated (by more than 2-fold) in stimulated Jurkat-HBZ cells identified by microarray analysis.

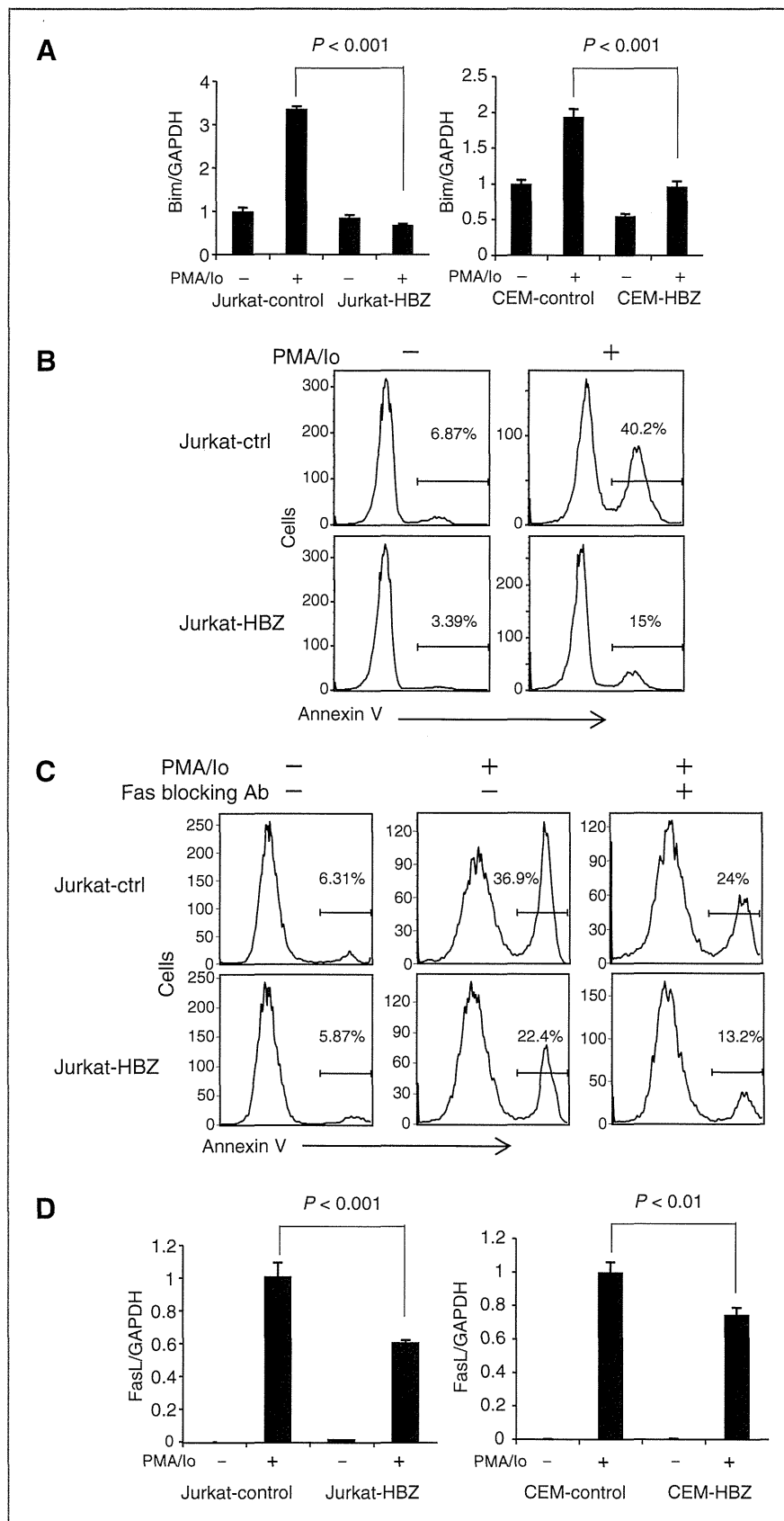


Figure 1. HBZ suppresses the transcription of the *Bim* and *FasL* genes and consequently stimulation-induced apoptosis. A, comparison of the *Bim* mRNA expression in the Jurkat-control, Jurkat-HBZ, CEM-control, and CEM-HBZ cells with or without PMA/Io stimulation by real-time PCR. B, Jurkat-control and Jurkat-HBZ were stimulated with PMA/Io for 9 hours and stained with Annexin V. Percentage of apoptotic cells was determined by flow cytometry. C, Jurkat-control and Jurkat-HBZ were treated with Fas-blocking antibody for 30 minutes and then stimulated with PMA/Io for 9 hours. Percentages of apoptotic cells were monitored by flow cytometry. D, comparison of the *FasL* mRNA transcription in the Jurkat-control, Jurkat-HBZ, CEM-control, and CEM-HBZ cells with or without PMA/Io stimulation by real-time PCR. Error bars, standard deviation. Statistical differences are calculated by Student *t* test. GAPDH, glyceraldehyde-3-phosphate dehydrogenase.

HBZ suppresses *Bim* expression through attenuation of FoxO3a

We analyzed how HBZ suppresses the expression of *Bim* and *FasL*. It has been reported that a forkhead factor, FoxO3a, and *p73* are important for the transcription of *Bim* and *FasL* (32, 33). FoxO3a and other FOXO family members are phosphorylated by protein kinases such as Akt or SGK on highly conserved serine and threonine residues (especially Thr32, Ser253, and Ser315 in FoxO3a), resulting in impaired DNA-binding activity and increased binding to the chaperone protein, 14-3-3 (20, 34, 35). Newly formed 14-3-3-FOXO complexes are then exported from the nucleus, thereby inhibiting FOXO-dependent transcription of key target genes such as *Bim*, *FasL*, and *TRAIL* (36).

First, we investigated whether FoxO3a is implicated for the activation induced cell death. As shown in Supplementary Fig. S2, the knockdown of FoxO3a resulted in the decreased apoptotic rate in Jurkat-control cells ($P < 0.05$). Furthermore, inhibition of Foxo3a did not influence activation-induced cell death in Jurkat-HBZ cells, suggesting the inhibitory effect of HBZ on Foxo3a function. To investigate whether HBZ affects FoxO3a function, Jurkat cells were transiently transfected with a plasmid expressing FoxO3aAAA, the constitutive active mutant of FoxO3a, which is no longer phosphorylated by Akt and is localized in the nucleus. The FoxO3aAAA was expressed together with hrGFP using an internal ribosome entry site (IRES; FoxO3aAAA-IRES-hrGFP). Jurkat cells were transiently transfected with full-length HBZ or its mutants. HBZ has three domains, an activation domain (AD), a central domain (CD), and a basic leucine zipper domain (bZIP; ref. 12). In this study, the deletion mutants (HBZ- Δ AD, HBZ- Δ bZIP, and HBZ- Δ CD) were used. The percentage of FoxO3aAAA induced apoptotic cells in the absence of HBZ was 69.6% while it was suppressed by HBZ (40.6%; $P < 0.001$; Fig. 2A). We also found that an HBZ mutant without activation domain lacks the activity to inhibit FoxO3aAAA-induced apoptosis (Fig. 2A), indicating the significance of activation domain in suppression of FoxO3a-mediated apoptosis. It has been reported that LXXLL motif in FoxO3a binds to its coactivator CBP/p300 (37). Similarly, HBZ has LXXLL-like motifs located in the NH₂-terminal region, which bind to KIX domain of CBP/p300 (38). We speculated that the LXXLL-like motifs of HBZ might affect FoxO3aAAA function through KIX domain of CBP/p300. An HBZ mutant, which has substitutions in 27th and 28th residues (LL to AA) of LXXLL-like motif, lack the activity to suppress FoxO3aAAA-mediated apoptosis (Fig. 2B), indicating that LXXLL-like motif of HBZ is critical for suppression of FoxO3a-mediated apoptosis.

Next, we analyzed the effect of HBZ on a FoxO3a responsive reporter. As shown in Fig. 2C, HBZ suppressed FoxO3a-mediated transcriptional activity ($P < 0.01$). To check whether HBZ inhibits DNA binding of FoxO3a, 293T cells were transiently transfected with FoxO3aAAA and FoxO3a reporter, 6xDBE-Luc, together with or without HBZ. The interaction of FoxO3aAAA to FOXO-binding sites was analyzed by ChIP assay. As shown in Figure 2D, the interaction of FoxO3aAAA to the FOXO-binding sites was interfered by HBZ, suggesting that HBZ inhibits FoxO3a-mediated apoptosis through suppression

of the DNA binding of FoxO3a. To clarify the mechanism of HBZ-mediated FoxO3a inhibition, we examined interaction between HBZ and FoxO3a by the immunoprecipitation assay. It showed that HBZ interacted with FoxO3a (Fig. 2E and F). Experiments with FoxO3a deletion mutant revealed that HBZ interacted with the forkhead domain of FoxO3a (Fig. 2E). Analysis using HBZ deletion mutants showed that the central domain of HBZ interacted with FoxO3a (Fig. 2F).

HBZ inhibits nuclear export of phosphorylated form of FoxO3a

Next, we investigated the effect of HBZ on FoxO3a localization by confocal microscopy. We cotransfected 293FT cells with a plasmid expressing human wild-type FoxO3a (FoxO3aWT) protein and an HBZ-expressing plasmid. Consistent with previous reports, FoxO3a remained mainly in cytoplasm when cells were cotransfected with empty vector (Fig. 3A; refs. 20, 34). However, when it was expressed along with HBZ, FoxO3a was localized in both nucleus and cytoplasm (Fig. 3A). To determine whether mislocalized FoxO3a is phosphorylated (pFoxO3a) or not, we used anti-pFoxO3a antibody. Figure 3B and C demonstrated that nuclear-localized FoxO3a was phosphorylated in HBZ-expressing cells. Thereafter, we analyzed the localization of endogenous FoxO3a in HeLa and an ATL cell line, MT-1. Although pFoxO3a was localized widely both in cytoplasm and nucleus in HeLa cells, most pFoxO3a was localized in the nucleus in MT-1 (Fig. 3D), suggesting that endogenous HBZ inhibits the extranuclear translocation of pFoxO3a in this cell line. From the study of crystal structure of the human FoxO3a-DBD/DNA complex, it has been reported that phosphorylation at Ser253 causes a decrease on the DNA-binding ability (39). Abnormal localization of phosphorylated FoxO3a by HBZ might interfere the function of unphosphorylated FoxO3a in the nucleus. The abnormal localization of pFoxO3a prompted us to investigate whether HBZ bound to 14-3-3 along with FoxO3a, as 14-3-3 is a chaperon protein involved in nuclear-cytoplasm shuttling of FOXO family. As shown in Figure 3E, HBZ, FoxO3a, and 14-3-3 form a ternary complex. However, the binding of FoxO3a and 14-3-3 was not affected by HBZ (result of IP with anti-FLAG antibody and detected with anti-HA antibody).

As another possible mechanism for downregulation of *Bim* and *FasL*, we compared the transcription level of *p73* in Jurkat cells with and without HBZ expression. Activation of HBZ-expressing cells reduced transcription of *p73*, but the expression level of *p73* was variable among ATL cell lines (Supplementary Fig. S3A and S3B). We conclude that *p73* is not responsible for suppression of *Bim* expression in ATL cells.

Bim expression is suppressed in both ATL cell lines and ATL cases

HBZ has been shown to suppress *Bim* expression through two different mechanisms as revealed in this study. To analyze *Bim* expression in ATL cells, we studied *Bim* mRNA levels in non-ATL cell lines and ATL cell lines with or without PMA/Io stimulation, and found that the *Bim* gene transcript was upregulated in Jurkat and CCRF-CEM cells, but not in SupT1 after activation. However, *Bim* transcripts were not increased

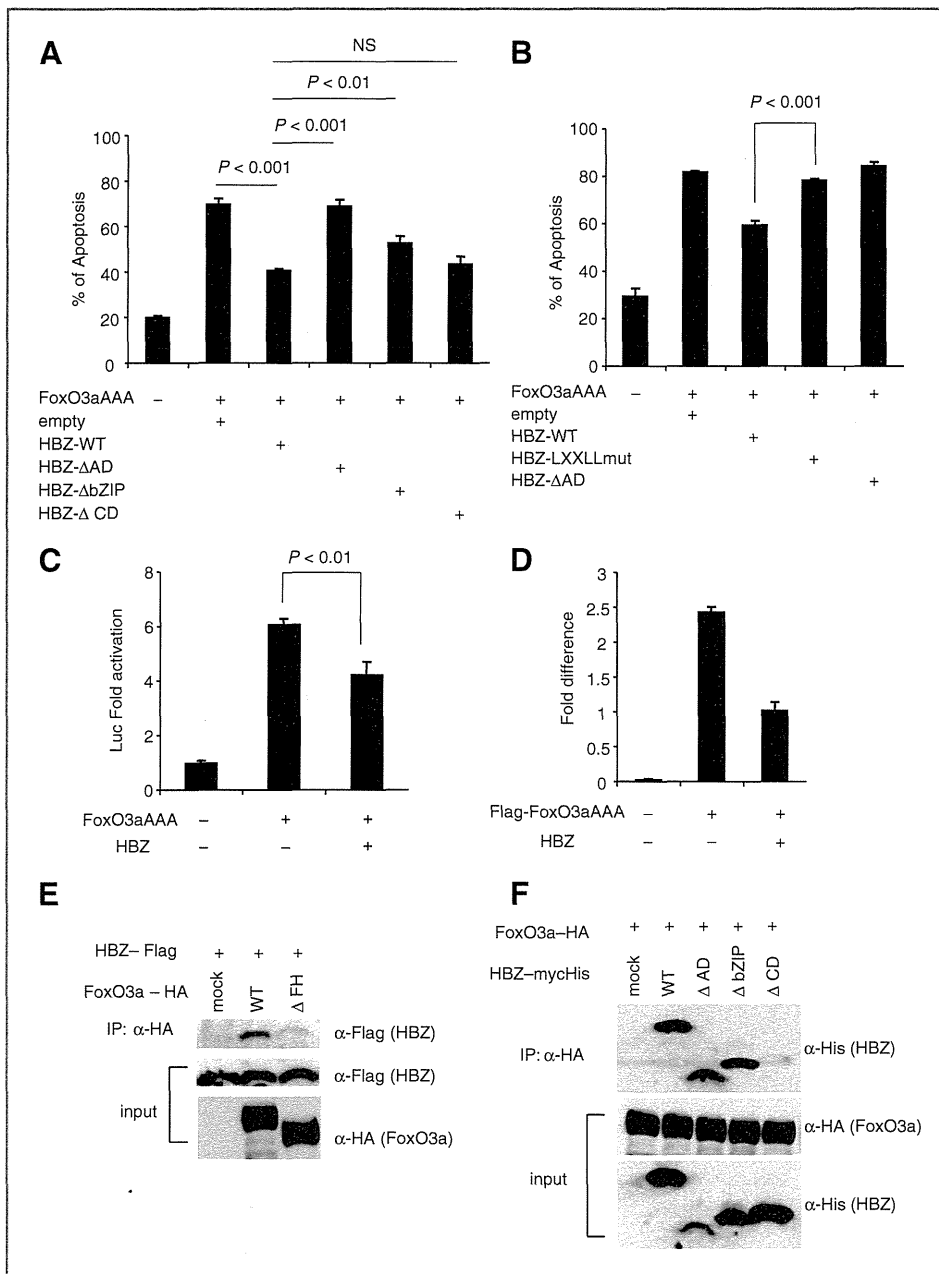


Figure 2. HBZ attenuates function of Foxo3a by physical interaction. A, Jurkat cells were transfected with FoxO3aAAA-expressing vector, a constitutively active form, by using Neon with or without HBZ or its mutants. Twenty-four hours after transfection, cells were stained with Annexin V and analyzed by flow cytometry ($n = 3$). B, Jurkat cells were transfected with FoxO3aAAA-expressing vector together with HBZ or its mutants by using Neon. Cells were stained with Annexin V and analyzed by flow cytometry ($n = 3$). Data are representative of three independent experiments. C, reporter construct containing the 6xDBE and FoxO3aAAA-expressing vector was transiently transfected with or without HBZ into Jurkat cells in the presence of Z-VAD-FMK and luciferase activities were measured. D, 293T cells were transfected with 6xDBE-Luc construct and Flag-tagged FoxO3aAAA expression vector together with or without HBZ expression vector. Cells were immunoprecipitated with anti-FLAG antibody and quantified by real-time PCR. Three independent ChIP experiments were done and representative data are shown. Error bars, experimental variation. E and F, the expression vectors of the indicated proteins were cotransfected into 293T cells, and their interactions were analyzed by immunoprecipitation assay. Data are representative of three independent experiments. Statistical differences are calculated by Student t test.

in all stimulated ATL cell lines (Fig. 4A). The *Bim* gene transcript was also downregulated in primary ATL cells (Fig. 4B) compared with resting peripheral blood mononuclear cells (PBMC) and phytohemagglutinin (PHA)-stimulated T cells. We also stimulated primary ATL cells and normal CD4⁺ T cells with PMA/Io. The *Bim* gene transcription was quite low in primary ATL sample compared with normal CD4⁺ T cells even though the cells were stimulated with PMA/Io (Fig. 4C). To confirm HBZ expression in representative ATL cell lines, we quantified the level of the *HBZ* mRNA transcription in Jurkat-HBZ, CEM-HBZ, MT-1, ED, and TL-Om1 by real-time PCR and confirmed that HBZ is expressed in these ATL cell lines (Supplementary Fig. S4). Microarray data, obtained from Gene

Expression Omnibus (GEO), show that both *Bim* and *FasL* transcription levels are lower in ATL cases than healthy donors (accession number: GSE33615; Supplementary Fig. S5), supporting our data that *Bim* expression was suppressed in ATL cells.

***Bim* expression is silenced by epigenetic mechanisms**

Because the *Bim* gene transcription was severely suppressed in ATL cells, we investigated the epigenetic status (DNA methylation and histone modification) of the promoter region of the *Bim* gene in ATL cells. A previous study showed that the 0.8 kb region immediately upstream of exon 1 contains the important elements for the control of *Bim* expression

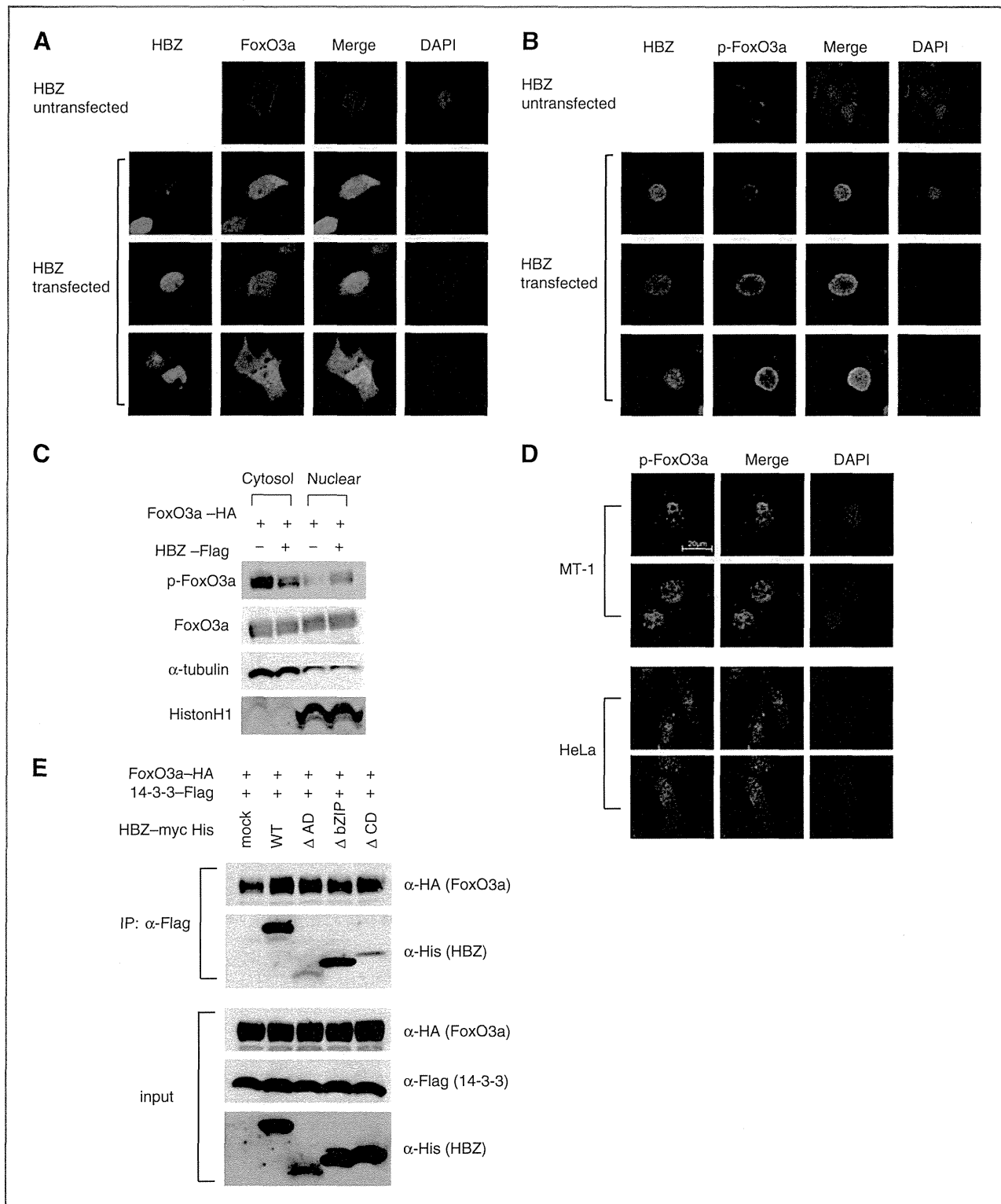


Figure 3. HBZ interferes with normal localization of FoxO3a by forming a ternary complex with FoxO3a and 14-3-3. 293FT cells were transfected with FoxO3aWT-Flag together with or without mycHis-HBZ. A and B, FoxO3a was detected using anti-FLAG-biotin and secondary Streptavidin-Alexa 488 (A), and p-FoxO3a was detected using anti-p-FoxO3a (ser253) and secondary anti-rabbit IgG-Alexa 488 antibody (B). DAPI was used to counterstain the nucleus. C, 293FT cells were transfected with HA-tagged FoxO3aWT together with or without Flag-tagged HBZ. Cytosolic and nuclear fractions were extracted and p-FoxO3a was detected by Western-blotting. D, endogenous localizations of p-FoxO3a (ser253) in HeLa and MT-1 cells were examined using anti-p-FoxO3a. E, the interactions among HBZ, FoxO3a, and 14-3-3 were analyzed by immunoprecipitation.

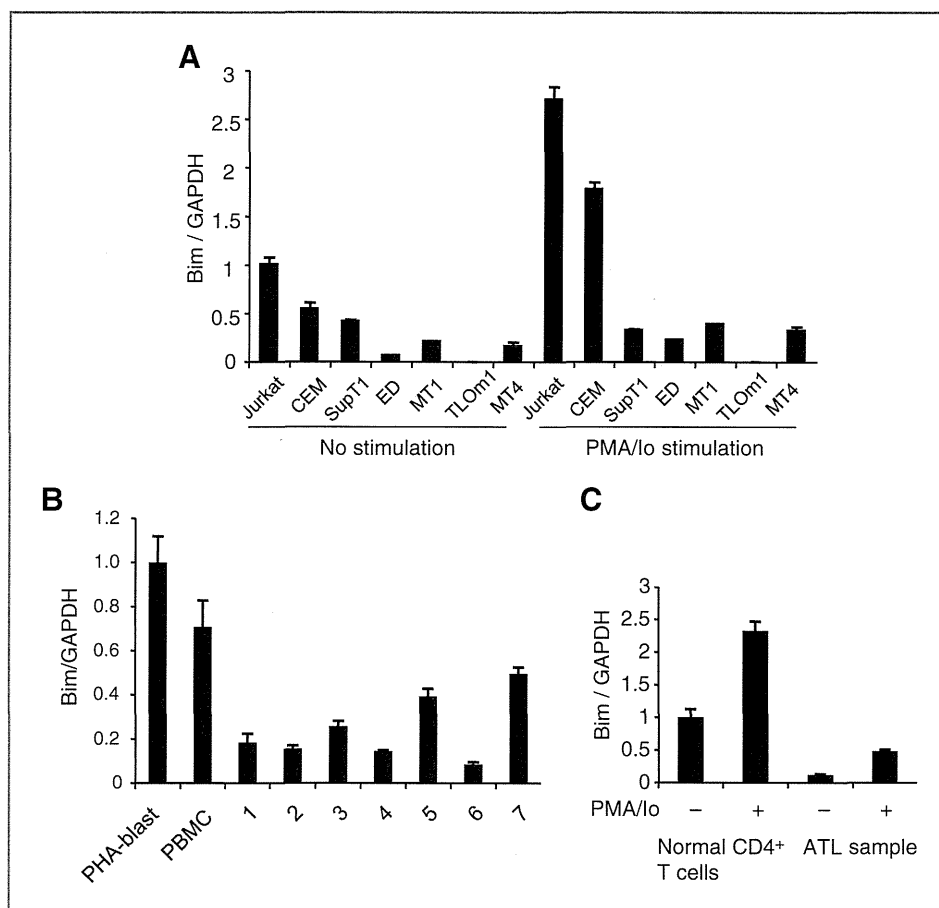


Figure 4. *Bim* expression is also suppressed in ATL cell lines and ATL cases. Comparison of the *Bim* mRNA expression in non-ATL cell lines and ATL cell lines with or without PMA/Io stimulation (A) and in PBMCs and PHA-blasts from healthy donor samples and fresh ATL samples (B) by real-time PCR. C, comparison of the *Bim* mRNA expression in healthy donor sample and ATL fresh sample with or without PMA/Io stimulation.

(promoter 1). The *Bim* promoter does not contain a TATA or CAAT box and has the characteristics of a "TATA-less" promoter (40). In addition, the alternative promoter has been reported to exist in intron 1 (promoter 2; refs. 41, 42). These two promoter regions are highly GC-rich and contain the binding sites for several transcription factors, including FoxO3a. To determine whether CpG sites in these *Bim* gene promoter regions are methylated in ATL cell lines, their methylation status was analyzed by bisulfite-mediated methylcytosine mapping (Supplementary Fig. S6A and S6B). The promoter 1 of *Bim* was hypermethylated in two ATL cell lines (ED and TL-Om1) and ATL case 1, whereas this region was not so methylated in MT-1 cells and two ATL cases. On the other hand, the promoter 2 was heavily methylated in two ATL cell lines (TL-Om1 and MT-1) and ATL case 1 and partially methylated in Jurkat cells (Supplementary Fig. S6B). These results suggest that in some cases, heavily methylated CpG sites of promoter 1 and 2 are associated with silencing of *Bim* transcription but these methylations can not account for suppressed *Bim* expression in all ATL cell lines and ATL cases.

Therefore, we next focused on the histone modification in the promoter region of *Bim*. It is well known that deacetylation of the histones are also common features of cancer, which results in transcriptional silencing of tumor suppressor genes (43). First, we analyzed the histone H3 and H4 acetylation and H3K4 trimethylation, which are all permissive marks (44), in

promoter 1 of Jurkat, MT-1, and TL-Om1 cells. Contrary to our speculation, neither H3, H4 acetylation, nor H3K4 trimethylation differed between MT-1 and Jurkat cells (Supplementary Fig. S7). We next analyzed the histone modification status in promoter 2. As shown in Figure 5A, MT-1 and TL-Om1 cells exhibited decreased level of histone H3 acetylation and H3K4 trimethylation but not histone H4 acetylation. Because methylation of DNA is often preceded by dimethylation of H3K9 or trimethylation of H3K27 (both repressive marks) in oncogenesis (44), we asked whether there were differences in these epigenetic chromatin marks on the *Bim* gene promoter in ATL cell lines. TL-Om1 cells exhibited upregulated level of H3K9 dimethylation and H3K27 trimethylation compared with Jurkat cells (Fig. 5B and C), whereas MT-1 exhibited a little upregulated level of H3K27 trimethylation (Fig. 5C) in the promoter 2. These data suggest that histone modifications of promoter 2 are critical for the suppressed *Bim* gene transcription. We also performed ChIP analysis using anti-RNA polymerase II antibody (Fig. 5D) and revealed that Pol II binding was decreased in MT-1 and TL-Om1 cells, confirming suppressed transcription of the *Bim* gene. To further investigate the mechanisms involved in FoxO3a-mediated *Bim* gene transcription in the promoter 2, we transfected HA-tagged FoxO3a expression vector together with or without a HBZ expression vector into 293T cells and immunoprecipitated with anti-HA antibody. Then, the DNA-binding capacity of FoxO3a was

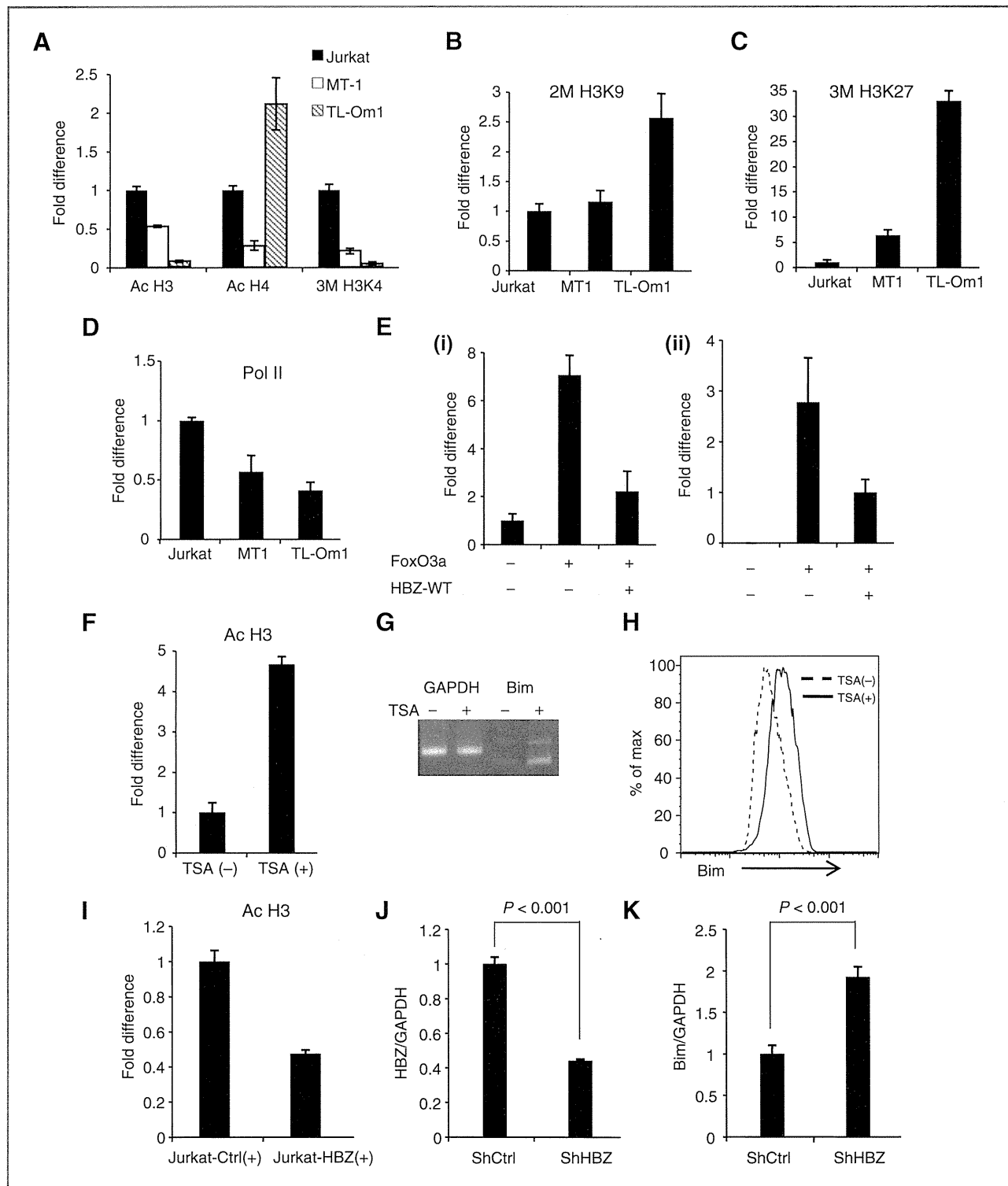


Figure 5. Epigenetic status of the promoter regions of the *Bim* gene. A–C, fold difference of acetylated histone H3, acetylated histone H4, trimethylated H3K4, dimethylated H3K9, or trimethylated H3K27; the data from Jurkat cells were arbitrarily set as 1.0. D, quantitative ChIP assay using RNA polymerase II (Pol II) antibody in Jurkat, MT-1, and TL-Om1 cells. E, 293T cells were transfected with HA-tagged FoxO3a expression vector together with or without HBZ expression vector. Cells were immunoprecipitated with anti-HA antibody and DNA-binding ability at promoter 2 was quantified by real-time PCR. F, fold difference of acetylated histone H3 in MT-1 cells, which were treated with or without 0.4 mmol/L TSA for 15 hours. The data from MT-1 cells without TSA treatment were arbitrarily set as 1.0. G and H, MT-1 cells were treated with 0.4 mmol/L TSA for 15 hours and *Bim* expression level was analyzed by quantitative real-time PCR and flow cytometry. I, fold difference of acetylated histone H3 in the *Bim* promoter in the Jurkat-control and Jurkat-HBZ cells 9 hours after the stimulation with PMA/I α . J, HBZ transcript in shRNA transfectant of MT-1 was quantified by real-time PCR. K, comparison of the *Bim* mRNA expression in control MT-1 cells and HBZ-KD MT-1 cells. Error bars, experimental variation. The data shown are representative of two or three independent experiments. Statistical differences are calculated by Student *t* test. GAPDH, glyceraldehyde-3-phosphate dehydrogenase.

quantified by real-time PCR. Figure 5E shows that HBZ attenuated the DNA-binding capacity of FoxO3a in the promoter 2 of *Bim* (i) and *FasL* promoter (ii), suggesting that the suppressed binding of FoxO3a to the promoter regions leads to inhibition of the *Bim* and *FasL* genes transcription by HBZ.

Next, we treated MT-1 cells with trichostatin A (TSA), a cell-permeable chemical inhibitor of class I/II histone deacetylases (HDAC). Treatment of TSA resulted in a clear upregulation of acetylation of histone H3 (Fig. 5F) followed by *Bim* expression both at the mRNA (Fig. 5G) and protein levels (Fig. 5H), indicating that histone modification is associated with suppressed *Bim* transcription in MT-1. We also performed ChIP assay using Jurkat-control and Jurkat-HBZ cells, which were stimulated with PMA and ionomycin for 9 hours, and found that acetylation of histone H3 decreased in Jurkat-HBZ cells (Fig. 5I), suggesting that HBZ is implicated in histone deacetylation in T cells. To verify whether HBZ inhibits transcription of the *Bim* gene, we suppressed the *HBZ* gene transcription by shRNA as reported previously (11). Efficiencies of lentivirus vector transduction, which were determined by EGFP expression, were 90.5% and 90.3% for control MT-1 cells and HBZ-knockdown MT-1 cells, respectively. Suppressed HBZ expression led to increase the *Bim* gene transcription (Fig. 5J and K), indicating that HBZ expression is linked to suppression of *Bim* expression in ATL cells.

Discussion

Human immunodeficiency virus type 1 (HIV-1) replicates vigorously and the generated virus infects target cells *in vivo*. Unlike HIV-1, HTLV-1 induces proliferation to increase the number of infected cells, as this virus is transmitted primarily by cell-to-cell contact (5). Therefore, HTLV-1-encoded proteins promote proliferation of infected cells and inhibit their apoptosis, resulting in an increased number of infected cells *in vivo* (2). In this study, we show that HBZ inhibits both the intrinsic and extrinsic apoptotic pathways via targeting FoxO3a, which leads to suppressed transcriptions of *Bim* and *FasL*. We demonstrated two mechanisms for perturbation of FoxO3a by HBZ: interaction of HBZ with FoxO3a and interference of nuclear export of phosphorylated FoxO3a. HBZ suppresses DNA-binding ability of active form of FoxO3a through interaction between central domain of HBZ and forkhead domain of FoxO3a. In addition, LXXLL-like motif of HBZ is implicated in inhibition of FoxO3a-mediated apoptosis, suggesting that HBZ interferes in interaction of CBP/p300 and FoxO3a. Furthermore, HBZ retains inactive form of FoxO3a in the nucleus through interaction with 14-3-3, leading to transcriptional repression of the target genes. Interestingly, accumulation of phosphorylated form of FoxO3a in the nucleus has been observed in HIV Vpr-expressing cells, which might be implicated in HIV-mediated resistance against insulin (28). Thus, FoxO3a is a target of both human retroviruses.

In this study, we showed that central domain of HBZ interacts with FoxO3a while LXXLL-like motif in activation domain of HBZ is responsible for suppressed apoptosis. LXXLL-like motif of HBZ has been reported to interact with KIX domain of p300 (38). The central domain of HBZ interacts

with the forkhead domain of FoxO3a, which binds to the target sequence (35). This is the mechanism how HBZ inhibits DNA binding of FoxO3a. However, inhibitory effect of HBZ on apoptosis largely depends on LXXLL-like motif of activation domain (Fig. 2A and B). FoxO3a is also reported to interact with KIX domain of CBP/p300 (37). Forkhead domain of FoxO3a intramolecularly interacts with its conserved regions (CR) 3, and binding of forkhead domain to DNA releases CR3, allowing it to bind KIX of CBP/p300 (45). These findings suggest that HBZ interferes in the complex interaction between FoxO3a and CBP/p300, which is likely important to induce apoptosis.

It has been reported that *Bim* has a tumor-suppressor function in various cancers. Hemizygous loss of the *Bim* gene promoted development of B-cell leukemia in Myc-transgenic mice in which c-myc expression was driven by the immunoglobulin gene intron-enhancer (46). Insulin-like growth factor 1 (IGF-1), an important growth factor for myeloma cells, has been reported to suppress *Bim* expression by epigenetic and posttranslational mechanisms (25). In Epstein-Barr virus-infected B cells, *Bim* transcription is silenced by DNA methylation of the *Bim* gene promoter (47). Thus, impaired expression of *Bim* is associated with the various cancers, including the virus-related malignancies. FoxO3a is also a target of oncogenesis. BCR-ABL induces phosphorylation of FoxO3a, which leads to suppressed expression of *Bim* in Ph1⁺ chronic myelogenous leukemia cells (32). In breast cancer, IκB kinase interacts with, phosphorylates FoxO3a, which causes proteolysis of FoxO3a (48). In this study, we revealed that HBZ hinders nuclear export of phosphorylated FoxO3a, and impairs function of FoxO3a likely through interaction of FoxO3a and p300. Thus, suppressed *Bim* and *FasL* expression through inhibition of FoxO3a by HBZ is a new mechanism for oncogenesis.

Besides FoxO3a perturbation by HBZ, we also have identified the epigenetic aberrations in the promoter region of the *Bim* gene in ATL cells, and found that *Bim* expression is suppressed by DNA methylation and histone modification. ATL cell lines exhibited upregulated level of H3K27 trimethylation in the promoter regions of *Bim*. It has been reported that enhancer of zeste (EZH) 2, a methyltransferase and component of the polycomb repressive complex 2, expression is increased in ATL cell lines (42). Because EZH2 plays an essential role in the epigenetic maintenance of H3K27 trimethylation, upregulated H3K27 trimethylation of the *Bim* gene promoter might be associated with increased expression of EZH2 in ATL cells. In addition, HBZ seems to be associated with histone deacetylation in MT-1 cells. According to the previous studies, it is known that both HBZ and FoxO3a bind to the histone acetyltransferase p300/CBP through the LXXLL motif (38). In this study, we found that the same motif is important for FoxO3a suppression and resulting inhibition of apoptosis. It is likely that HBZ decreases histone acetylation level on *Bim* promoter through the interaction with FoxO3a and dissociation of p300/CBP from the promoter. In addition to histone modifications, hypermethylation of CpGs in *Bim* promoter was observed in some ATL cells. These epigenetic aberrations likely occur as the secondary changes following long-time silencing of *Bim* by HBZ, although further investigations will be required.

In this study, we demonstrated that HBZ suppresses activation-induced apoptosis by downregulation of proapoptotic genes, *Bim* and *FasL*. HBZ perturbs the function of FoxO3a by interaction, and induces epigenetic aberrations in the promoter region of the *Bim* gene. It has been shown that HBZ induces not only cancer but also inflammation *in vivo*. Because inflammatory diseases are essentially caused by failure to negatively regulate unnecessary immune responses by apoptosis, suppression of apoptosis by HBZ might be associated with HTLV-1-induced inflammation as well. Collectively, HBZ-mediated inhibition of apoptosis is likely implicated in both neoplastic and inflammatory diseases caused by HTLV-1.

Disclosure of Potential Conflicts of Interest

No potential conflicts of interest were disclosed.

Authors' Contributions

Conception and design: A. Tanaka-Nakanishi, J. Yasunaga, M. Matsuoka
Development of methodology: A. Tanaka-Nakanishi, M. Matsuoka
Acquisition of data (provided animals, acquired and managed patients, provided facilities, etc.): A. Tanaka-Nakanishi, K. Takai

Analysis and interpretation of data (e.g., statistical analysis, biostatistics, computational analysis): A. Tanaka-Nakanishi, J. Yasunaga, K. Takai, M. Matsuoka

Writing, review, and/or revision of the manuscript: A. Tanaka-Nakanishi, J. Yasunaga, M. Matsuoka

Administrative, technical, or material support (i.e., reporting or organizing data, constructing databases): M. Matsuoka

Study supervision: M. Matsuoka

Acknowledgments

The authors thank T. Furuyama (Kagawa Prefectural University of Health Science) for the 6xDBE-Luc plasmid DNA, P. Bouillet for valuable comments on this study, and L. Kingsbury for proofreading of this manuscript.

Grant Support

This study was supported by a Grant-in-aid for Scientific Research from the Ministry of Education, Science, Sports, and Culture of Japan to M. Matsuoka (MEXT grant number 221S0001), a grant from Japan Leukemia Research Fund to M. Matsuoka, and a grant from the Takeda Science Foundation to J. Yasunaga.

The costs of publication of this article were defrayed in part by the payment of page charges. This article must therefore be hereby marked *advertisement* in accordance with 18 U.S.C. Section 1734 solely to indicate this fact.

Received February 14, 2013; revised September 12, 2013; accepted October 5, 2013; published OnlineFirst October 31, 2013.

References

- Proietti FA, Carneiro-Proietti AB, Catalan-Soares BC, Murphy EL. Global epidemiology of HTLV-I infection and associated diseases. *Oncogene* 2005;24:6058–68.
- Matsuoka M, Jeang KT. Human T-cell leukaemia virus type 1 (HTLV-1) infectivity and cellular transformation. *Nat Rev Cancer* 2007;7:270–80.
- Igakura T, Stinchcombe JC, Goon PK, Taylor GP, Weber JN, Griffiths GM, et al. Spread of HTLV-I between lymphocytes by virus-induced polarization of the cytoskeleton. *Science* 2003;299:1713–6.
- Pais-Correia AM, Sachse M, Guadagnini S, Robbiati V, Lasserre R, Gessain A, et al. Biofilm-like extracellular viral assemblies mediate HTLV-1 cell-to-cell transmission at virological synapses. *Nat Med* 2010;16:83–9.
- Derse D, Hill SA, Lloyd PA, Chung H, Morse BA. Examining human T-lymphotropic virus type 1 infection and replication by cell-free infection with recombinant virus vectors. *J Virol* 2001;75:8461–8.
- Mazurov D, Ilinskaya A, Heidecker G, Lloyd P, Derse D. Quantitative comparison of HTLV-1 and HIV-1 cell-to-cell infection with new replication dependent vectors. *PLoS Pathog* 2010;6:e1000788.
- Cavrois M, Leclercq I, Gout O, Gessain A, Wain-Hobson S, Wattel E. Persistent oligoclonal expansion of human T-cell leukemia virus type 1-infected circulating cells in patients with Tropical spastic paraparesis/HTLV-1 associated myelopathy. *Oncogene* 1998;17:77–82.
- Etoh K, Tamiya S, Yamaguchi K, Okayama A, Tsubouchi H, Ideta T, et al. Persistent clonal proliferation of human T-lymphotropic virus type I-infected cells *in vivo*. *Cancer Res* 1997;57:4862–7.
- Grassmann R, Aboud M, Jeang KT. Molecular mechanisms of cellular transformation by HTLV-1 Tax. *Oncogene* 2005;24:5976–85.
- Fan J, Ma G, Nosaka K, Tanabe J, Satou Y, Koito A, et al. APOBEC3G generates nonsense mutations in HTLV-1 proviral genomes *in vivo*. *J Virol* 2010;84:7278–87.
- Satou Y, Yasunaga J, Yoshida M, Matsuoka M. HTLV-I basic leucine zipper factor gene mRNA supports proliferation of adult T cell leukemia cells. *Proc Natl Acad Sci U S A* 2006;103:720–5.
- Satou Y, Yasunaga J, Zhao T, Yoshida M, Miyazato P, Takai K, et al. HTLV-1 bZIP factor induces T-cell lymphoma and systemic inflammation *in vivo*. *PLoS Pathog* 2011;7:e1001274.
- Bouillet P, O'Reilly LA. CD95, BIM and T cell homeostasis. *Nat Rev Immunol* 2009;9:514–9.
- Debatin KM, Goldman CK, Waldmann TA, Krammer PH. APO-1-induced apoptosis of leukemia cells from patients with adult T-cell leukemia. *Blood* 1993;81:2972–7.
- Yasunaga J, Taniguchi Y, Nosaka K, Yoshida M, Satou Y, Sakai T, et al. Identification of aberrantly methylated genes in association with adult T-cell leukemia. *Cancer Res* 2004;64:6002–9.
- Krueger A, Fas SC, Giaisi M, Bleumink M, Merling A, Stumpf C, et al. HTLV-1 Tax protects against CD95-mediated apoptosis by induction of the cellular FLICE-inhibitory protein (c-FLIP). *Blood* 2006;107:3933–9.
- Okamoto K, Fujisawa J, Reth M, Yonehara S. Human T-cell leukemia virus type-I oncoprotein Tax inhibits Fas-mediated apoptosis by inducing cellular FLIP through activation of NF-kappaB. *Genes Cells* 2006;11:177–91.
- Sun SC, Yamaoka S. Activation of NF-kappaB by HTLV-I and implications for cell transformation. *Oncogene* 2005;24:5952–64.
- Zhao T, Yasunaga J, Satou Y, Nakao M, Takahashi M, Fujii M, et al. Human T-cell leukemia virus type 1 bZIP factor selectively suppresses the classical pathway of NF-kappaB. *Blood* 2009;113:2755–64.
- Brunet A, Bonni A, Zigmund MJ, Lin MZ, Juo P, Hu LS, et al. Akt promotes cell survival by phosphorylating and inhibiting a Forkhead transcription factor. *Cell* 1999;96:857–68.
- Zhao T, Satou Y, Sugata K, Miyazato P, Green PL, Imamura T, et al. HTLV-1 bZIP factor enhances TGF- β signaling through p300 coactivator. *Blood* 2011;118:1865–76.
- Furuyama T, Nakazawa T, Nakano I, Mori N. Identification of the differential distribution patterns of mRNAs and consensus binding sequences for mouse DAF-16 homologues. *Biochem J* 2000;349:629–34.
- Ponchel F, Toomes C, Bransfield K, Leong FT, Douglas SH, Field SL, et al. Real-time PCR based on SYBR-Green I fluorescence: an alternative to the TaqMan assay for a relative quantification of gene rearrangements, gene amplifications and micro gene deletions. *BMC Biotechnol* 2003;3:18.
- Richter-Larrea JA, Robles EF, Fresquet V, Beltran E, Rullan AJ, Agirre X, et al. Reversion of epigenetically mediated BIM silencing overcomes chemoresistance in Burkitt lymphoma. *Blood* 2010;116:2531–42.
- De Bruyne E, Bos TJ, Schuit F, Van Valckenborgh E, Menu E, Thorrez L, et al. IGF-1 suppresses Bim expression in multiple myeloma via epigenetic and posttranslational mechanisms. *Blood* 2010;115:2430–40.
- Fan J, Kodama E, Koh Y, Nakao M, Matsuoka M. Halogenated thymidine analogues restore the expression of silenced genes without demethylation. *Cancer Res* 2005;65:6927–33.

27. Kumaki Y, Oda M, Okano M. QUMA: quantification tool for methylation analysis. *Nucleic Acids Res* 2008;36:W170–5.
28. Kino T, De Martino MU, Charmandari E, Ichijo T, Outas T, Chrousos GP. HIV-1 accessory protein Vpr inhibits the effect of insulin on the Foxo subfamily of forkhead transcription factors by interfering with their binding to 14-3-3 proteins: potential clinical implications regarding the insulin resistance of HIV-1-infected patients. *Diabetes* 2005;54:23–31.
29. Cante-Barrett K, Gallo EM, Winslow MM, Crabtree GR. Thymocyte negative selection is mediated by protein kinase C- and Ca²⁺-dependent transcriptional induction of bim [corrected]. *J Immunol* 2006;176:2299–306.
30. Snow AL, Oliveira JB, Zheng L, Dale JK, Fleisher TA, Lenardo MJ. Critical role for BIM in T cell receptor restimulation-induced death. *Biol Direct* 2008;3:34.
31. Green DR, Droin N, Pinkoski M. Activation-induced cell death in T cells. *Immunol Rev* 2003;193:70–81.
32. Essafi A, Fernandez de Mattos S, Hassen YA, Soeiro I, Mufti GJ, Thomas NS, et al. Direct transcriptional regulation of Bim by FoxO3a mediates STI571-induced apoptosis in Bcr-Abl-expressing cells. *Oncogene* 2005;24:2317–29.
33. Busuttill V, Droin N, McCormick L, Bernassola F, Candi E, Melino G, et al. NF-kappaB inhibits T-cell activation-induced, p73-dependent cell death by induction of MDM2. *Proc Natl Acad Sci U S A* 2010;107:18061–6.
34. Brunet A, Park J, Tran H, Hu LS, Hemmings BA, Greenberg ME. Protein kinase SGK mediates survival signals by phosphorylating the forkhead transcription factor FKHL1 (FOXO3a). *Mol Cell Biol* 2001;21:952–65.
35. Obsil T, Obsilova V. Structure/function relationships underlying regulation of FOXO transcription factors. *Oncogene* 2008;27:2263–75.
36. Modur V, Nagarajan R, Evers BM, Milbrandt J. FOXO proteins regulate tumor necrosis factor-related apoptosis inducing ligand expression. Implications for PTEN mutation in prostate cancer. *J Biol Chem* 2002;277:47928–37.
37. Wang F, Marshall CB, Yamamoto K, Li GY, Gasmi-Seabrook GM, Okada H, et al. Structures of KIX domain of CBP in complex with two FOXO3a transactivation domains reveal promiscuity and plasticity in coactivator recruitment. *Proc Natl Acad Sci U S A* 2012;109:6078–83.
38. Clerc I, Polakowski N, Andre-Arpin C, Cook P, Barbeau B, Mesnard JM, et al. An interaction between the human T cell leukemia virus type 1 basic leucine zipper factor (HBZ) and the KIX domain of p300/CBP contributes to the down-regulation of tax-dependent viral transcription by HBZ. *J Biol Chem* 2008;283:23903–13.
39. Tsai KL, Sun YJ, Huang CY, Yang JY, Hung MC, Hsiao CD. Crystal structure of the human FOXO3a-DBD/DNA complex suggests the effects of post-translational modification. *Nucleic Acids Res* 2007;35:6984–94.
40. Bouillet P, Zhang LC, Huang DC, Webb GC, Bottema CD, Shore P, et al. Gene structure alternative splicing, and chromosomal localization of pro-apoptotic Bcl-2 relative Bim. *Mamm Genome* 2001;12:163–8.
41. Gilley J, Ham J. Evidence for increased complexity in the regulation of Bim expression in sympathetic neurons: involvement of novel transcriptional and translational mechanisms. *DNA Cell Biol* 2005;24:563–73.
42. Gilley J, Coffey PJ, Ham J. FOXO transcription factors directly activate bim gene expression and promote apoptosis in sympathetic neurons. *J Cell Biol* 2003;162:613–22.
43. Marks P, Rifkin RA, Richon VM, Breslow R, Miller T, Kelly WK. Histone deacetylases and cancer: causes and therapies. *Nat Rev Cancer* 2001;1:194–202.
44. Fullgrabe J, Kavanagh E, Joseph B. Histone onco-modifications. *Oncogene* 2011;30:3391–403.
45. Wang F, Marshall CB, Li GY, Yamamoto K, Mak TW, Ikura M. Synergistic interplay between promoter recognition and CBP/p300 coactivator recruitment by FOXO3a. *ACS Chem Biol* 2009;4:1017–27.
46. Egle A, Harris AW, Bouillet P, Cory S. Bim is a suppressor of Myc-induced mouse B cell leukemia. *Proc Natl Acad Sci U S A* 2004;101:6164–9.
47. Paschos K, Smith P, Anderton E, Middeldorp JM, White RE, Allday MJ. Epstein-barr virus latency in B cells leads to epigenetic repression and CpG methylation of the tumour suppressor gene Bim. *PLoS Pathog* 2009;5:e1000492.
48. Hu MC, Lee DF, Xia W, Golfman LS, Ou-Yang F, Yang JY, et al. IkkappaB kinase promotes tumorigenesis through inhibition of forkhead FOXO3a. *Cell* 2004;117:225–37.

Cancer Research

The Journal of Cancer Research (1916–1930) | The American Journal of Cancer (1931–1940)

HTLV-1 bZIP Factor Suppresses Apoptosis by Attenuating the Function of FoxO3a and Altering Its Localization

Azusa Tanaka-Nakanishi, Jun-ichirou Yasunaga, Ken Takai, et al.

Cancer Res 2014;74:188-200. Published OnlineFirst October 31, 2013.

Updated version Access the most recent version of this article at:
[doi:10.1158/0008-5472.CAN-13-0436](https://doi.org/10.1158/0008-5472.CAN-13-0436)

Supplementary Material Access the most recent supplemental material at:
<http://cancerres.aacrjournals.org/content/suppl/2013/10/31/0008-5472.CAN-13-0436.DC1.html>

Cited Articles This article cites by 48 articles, 24 of which you can access for free at:
<http://cancerres.aacrjournals.org/content/74/1/188.full.html#ref-list-1>

E-mail alerts Sign up to receive free email-alerts related to this article or journal.

Reprints and Subscriptions To order reprints of this article or to subscribe to the journal, contact the AACR Publications Department at pubs@aacr.org.

Permissions To request permission to re-use all or part of this article, contact the AACR Publications Department at permissions@aacr.org.

CASE STUDY

Open Access

A case of post-transplant adult T-cell leukemia/lymphoma presenting myelopathy similar to but distinct from human T-cell leukemia virus type I (HTLV-I)-associated myelopathy

Toyotaka Kawamata^{1*}, Nobuhiro Ohno¹, Kota Sato^{1,2}, Masayuki Kobayashi^{1,2}, Norihide Jo¹, Koichiro Yuji¹, Ryuji Tanosaki³, Yoshihisa Yamano⁴, Arinobu Tojo^{1,2} and Kaoru Uchimaru¹

Abstract

Introduction: Adult T-cell leukemia/lymphoma (ATL) responds poorly to conventional chemotherapy, but allogeneic stem cell transplantation (allo-SCT) may improve disease prognosis. Herein, we report a female patient with human T-cell leukemia virus type I (HTLV-I)-associated myelopathy (HAM)-like myelopathy following allo-SCT for ATL.

Case report: She developed crural paresis 14 months after allo-SCT. Initially, she was diagnosed with central nervous system (CNS) relapse of ATL and treated with intrathecal injection and whole brain and spine irradiation. Her symptoms recurred 5 months later, when a cerebrospinal fluid (CSF) specimen showed increased CD4 + CXCR3 + CCR4+ cell numbers and levels of neopterin and CXCL10 (IP-10).

Discussion: These results suggest the possible involvement of a certain immunological mechanism such as HAM in her symptoms, irrespective of the lack of anti-HTLV-I antibody in her CSF. Because a definitive diagnosis of CNS manifestation of ATL is sometimes difficult, multi-modal laboratory data are required for differential diagnosis.

Keywords: Adult T-cell leukemia/lymphoma; Post-transplant myelopathy; HTLV-I-associated myelopathy (HAM); Neopterin; CXCL10 (IP-10)

Introduction

Human T-cell leukemia virus type I (HTLV-I) was the first retrovirus identified in humans, isolated from a patient with cutaneous lymphoma (Poesz et al. 1980). HTLV-I is the cause of not only adult T-cell leukemia/lymphoma (ATL) (Uchiyama et al. 1977; Hinuma et al. 1981) but also HTLV-I-associated myelopathy (HAM)/tropical spastic paraparesis (TSP) (Osame et al. 1986), HTLV-I-associated uveitis (HU) (Ohba et al. 1989; Mochizuki et al. 1992) and infective dermatitis (McGill et al. 2012; de Oliveira et al. 2010).

ATL is one of the most intractable T-cell malignancies, and it responds poorly to conventional chemotherapy, with a median survival time (MST) of approximately

8 months (Shimoyama et al. 1988). Among such treatments, modified LSG-15 (mLSG-15) has shown the best results; in a previous study, the progression free survival (PFS) at 1 year among patients treated with mLSG-15 was 28% and the overall survival (OS) at 3 years was 24% (Tsukasaka et al. 2007). However, the improvement in survival time by mLSG-15 treatment is not satisfactory. Allo-HSCT is a promising treatment option to cure ATL because it may improve disease prognosis (Utsunomiya et al. 2001; Kami et al. 2003).

Herein, we describe a case of HAM-like myelopathy that was difficult to distinguish from central nervous system (CNS) relapse of ATL following allogeneic peripheral blood stem cell transplantation. This case report suggests that there might be immunological myelopathy after HSCT. In the present case, flow cytometric analysis of the cells in cerebrospinal fluid (CSF) was helpful to differentiate it from CNS relapse of ATL.

* Correspondence: toyotaka@ims.u-tokyo.ac.jp

¹Department of Hematology/Oncology, Research Hospital, The Institute of Medical Science, the University of Tokyo, 4-6-1 Shirokanedai, Minato-ku, Tokyo 108-8639, Japan

Full list of author information is available at the end of the article

Case report

A 63-year-old female patient recognized cervical lymph nodes swelling in October 2010. Lactate dehydrogenase (LDH) and serum corrected calcium levels kept within normal limit, but soluble interleukin-2 receptor (sIL-2R) elevated significantly at the initial visit (Table 1). Diagnostic imaging by computed tomography (CT) revealed systemic lymphadenopathies (cervical, axial, mediastinal, abdominal and mesenteric lymphadenopathy) before the following chemotherapy. Although appetite loss and abdominal distention were added with lymphadenopathy, any other abnormal finding of physical examination could not be detected. Her ECOG performance status was grade 1 before chemotherapy. She received cervical lymph node biopsy and pathological findings of cervical lymph node revealed T cell lymphoma compatible, and HTLV-I provirus DNA analysis (Southern blot) revealed monoclonal integration. Abnormal lymphocytes were not detected in peripheral blood (PB) and HTLV-I provirus DNA analysis of PB did not show monoclonal integration. She was diagnosed as ATL (lymphoma type). She has past histories of glaucoma and pulmonary cryptococcosis. None of ATL patient was in her family.

She was referred to our hospital and received four sessions of mLSG-15 therapy in our hospital. Prophylactic intrathecal injection was performed twice, during chemotherapy and before allogeneic stem cell transplantation. No meningeal involvement of ATL cells was detected at that time. She went into complete remission (Response criteria for adult T cell leukemia-lymphoma from an international consensus meeting (Tsukasaki et al. 2009)) in April 2011. She received following allogeneic peripheral blood stem cell transplantation (allo-PBSCT) in the National Cancer Center Hospital (Tokyo, Japan) (Figure 1). The transplantation conditioning regimen consisted of

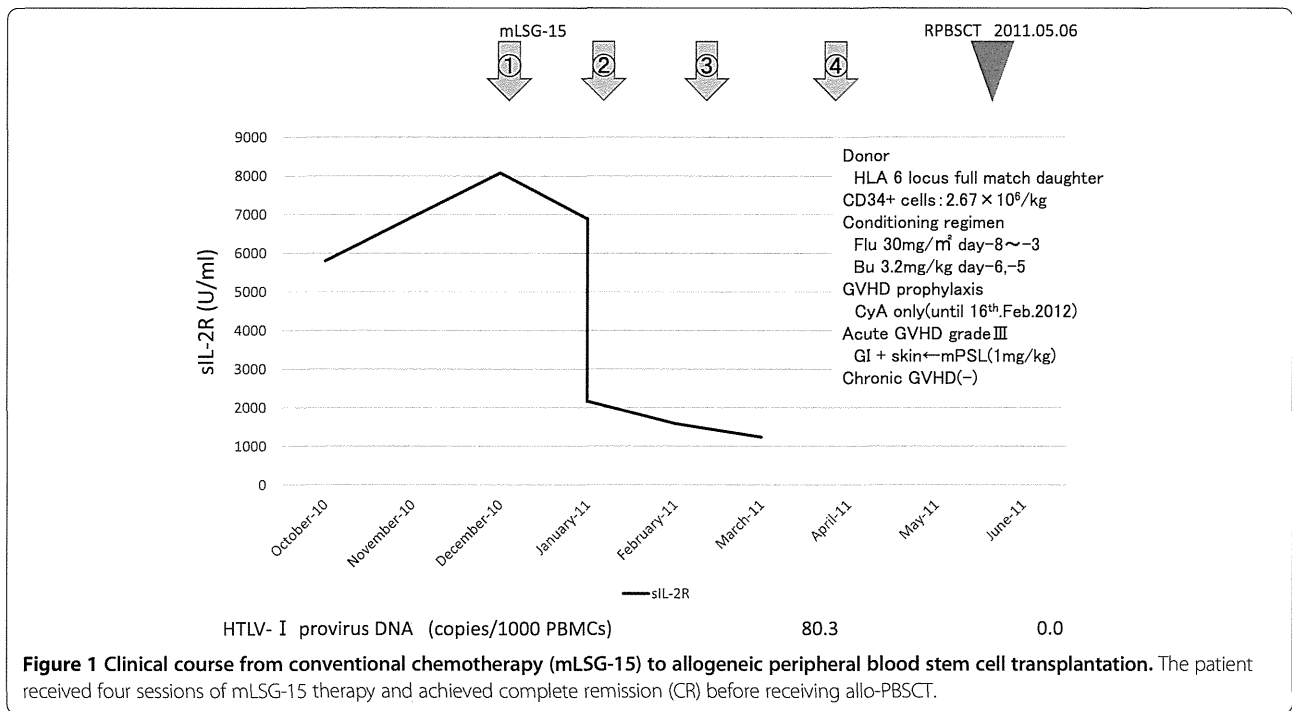
fludarabine (30 mg/m² per day for 5 days) plus busulfan (3.2 mg/kg per day for 2 days) and only cyclosporine A (CyA) was used for GVHD prophylaxis. Transplanted CD34-positive cells were 2.67 × 10⁶/kg and rapid engraftment was achieved. Grade III (gastrointestinal tract and skin) acute graft-versus-host disease (GVHD) was observed 1 month after transplantation, but it improved after treatment with methylprednisolone (mPSL) (1 mg/kg). No chronic GVHD was observed. CyA was tapered gradually and discontinued 9 months after transplantation, in February 2012. After that point, only 5 mg/day prednisolone (PSL) was continued.

In July 2012 (14 months after allo-PBSCT), the patient developed hemiparesis of the left side. Although left upper-limb paresis improved, lower-extremity paresis progressed to paraplegia. Magnetic resonance imaging (MRI) revealed multiple high-intensity lesions in T2-weighted images of the medulla oblongata, cervical spinal cord, and thoracic spinal cord (Figure 2A), and a CSF specimen showed increased cell counts (Figure 3). Morphologically, typical ATL cells such as flower cells were not detected in CSF, but abnormal small to middle size lymphocytes indistinguishable from ATL cells increased. She was diagnosed as CNS relapse of ATL, and received mPSL pulse, intrathecal injection of MTX 15 mg + Ara-C 40 mg + PSL 20 mg, and irradiation of the whole brain and spine. Following these treatments, the paraplegia improved gradually to such a degree that she could walk with a walker. During the course of these treatments, she was complicated by neurogenic bladder dysfunction, and diabetes insipidus.

In January 2013 (20 months after allo-PBSCT), she again developed left lower-limb weakness, which gradually progressed. She was admitted to our hospital in February 2013. On admission, neurological examination revealed

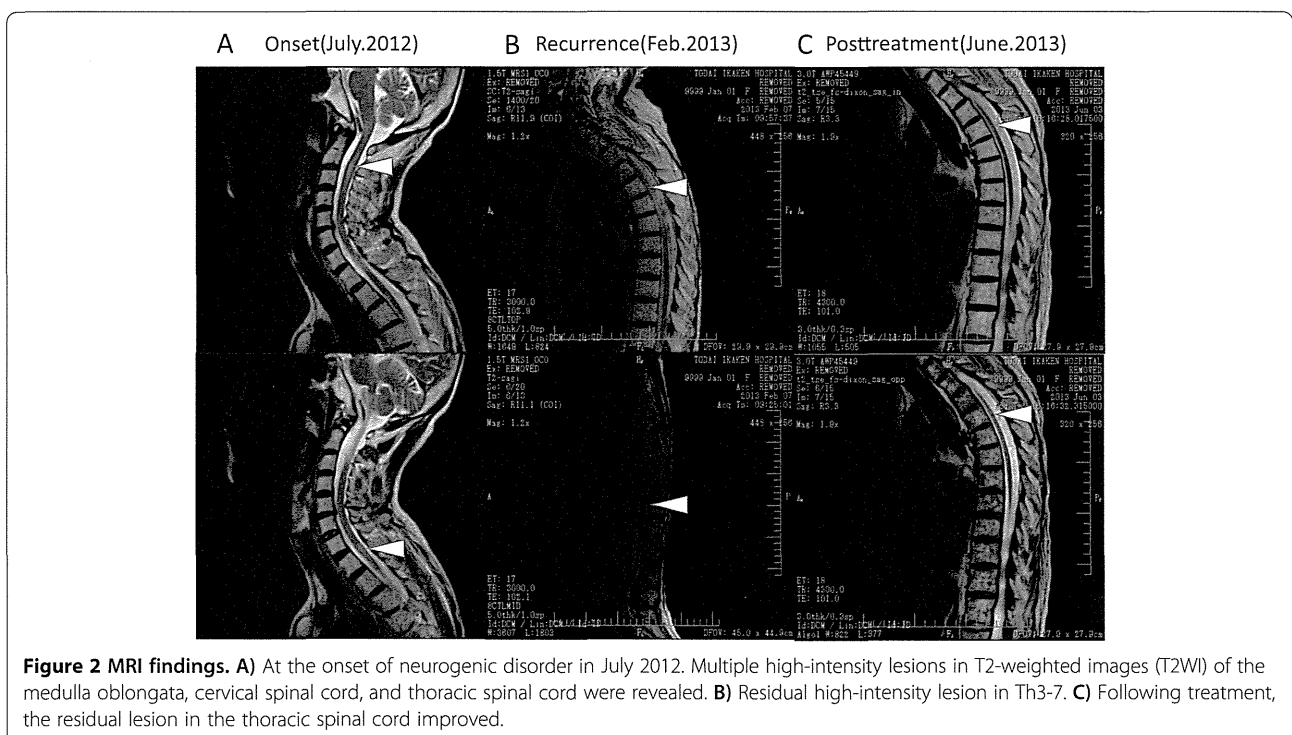
Table 1 Laboratory data of onset of ATL (lymphoma type) in October 2010

WBC	4100/μl	GOT	67 IU/L	CRP	0.06 mg/dl
Myelo	1.0%	GPT	72 IU/L	sIL-2R	5802 U/ml
St	8.0%	LDH	215 IU/L		
Seg	71.0%	ALP	277 IU/L	HTVL-I Ab	(+)
Ly	11.0%	γ-GTP	46 IU/L	HBs-Ag	(-)
Mo	8.0%	Alb	3.5 mg/dl	HBs-Ab	(-)
Baso	1.0%	BUN	15.6 mg/dl	HBc-Ab	(-)
RBC	423 × 10 ⁴ /μl	Cre	0.58 mg/dl	HCV-Ab	(-)
Hb	13.2 g/dl	Na	142.4 mEq/L	HIV-Ab	(-)
Hct	39.0%	K	4.2 mEq/L	TPHA	(-)
MCV	92.2 fl	Cl	103.8 mEq/L		
MCH	31.2 pg	Corrected Ca	9.9 mg/dl		
MCHC	33.8%				
Plt	21.9 × 10 ⁴ /μl				



no abnormality of cranial nervous system, but abnormal reflex such as Babinski and Chaddock reflex in bilateral lower-limb. Thermal hypoalgesia under right Th4 and left Th6 dermatome was detected, but tactile sense was intact. She was accompanied with bladder dysfunction and severe constipation. Brain and spinal MRI revealed a residual

spinal lesion at Th3-7 (Figure 2B). The cell numbers in CSF did not increase, but myelin basic protein (MBP) level was elevated (Figure 4B). Morphologically, ATL cells could not be detected in CSF. Flow cytometric analysis to determine the specific immunophenotype of CD4+ lymphocytes in CSF revealed an expansion of the CD4⁺CXCR3⁺CCR4⁺



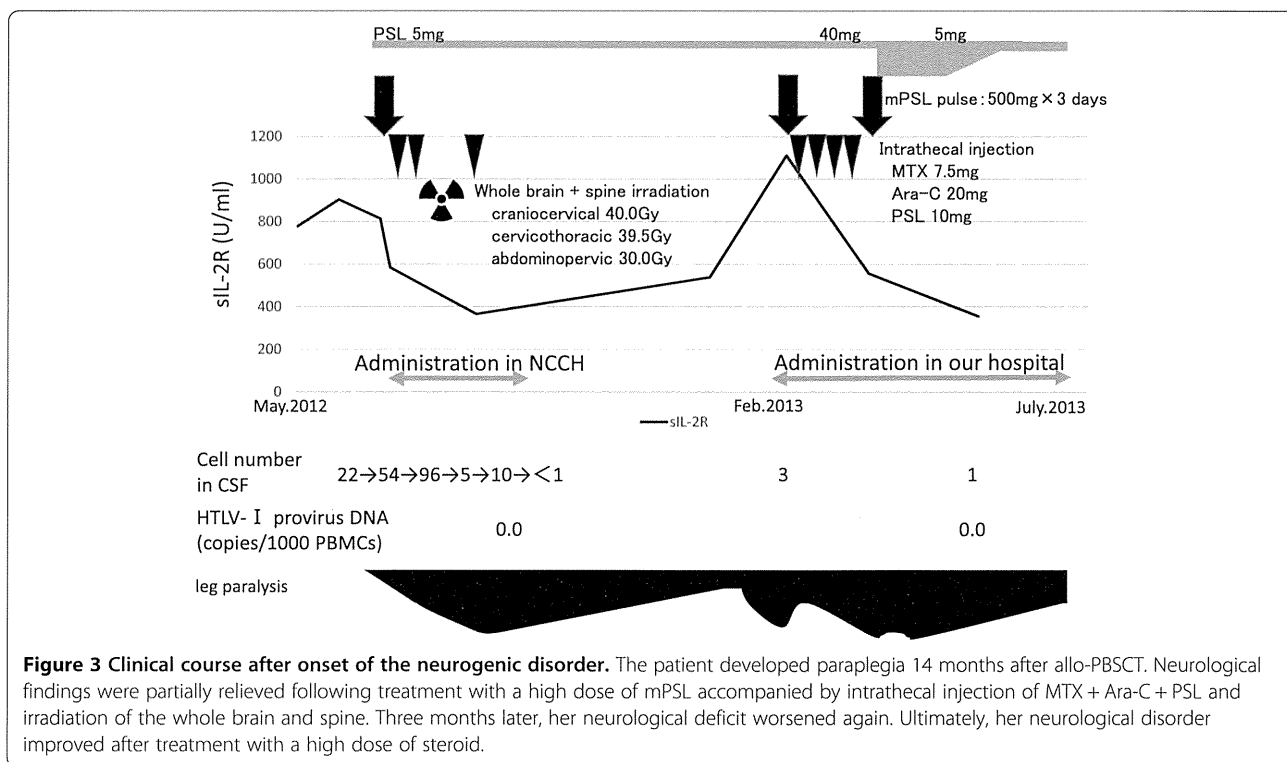


Figure 3 Clinical course after onset of the neurogenic disorder. The patient developed paraplegia 14 months after allo-PBSCT. Neurological findings were partially relieved following treatment with a high dose of mPSL accompanied by intrathecal injection of MTX + Ara-C + PSL and irradiation of the whole brain and spine. Three months later, her neurological deficit worsened again. Ultimately, her neurological disorder improved after treatment with a high dose of steroid.

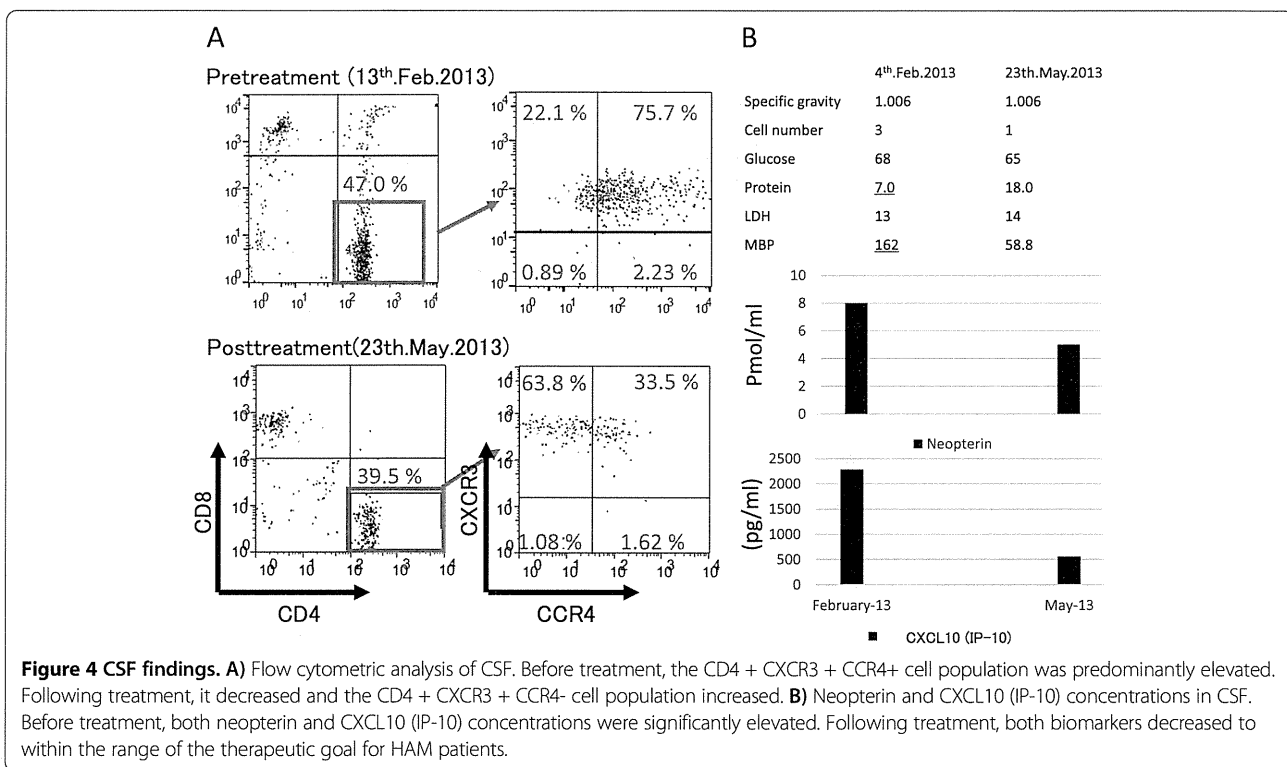


Figure 4 CSF findings. A) Flow cytometric analysis of CSF. Before treatment, the CD4 + CXCR3 + CCR4+ cell population was predominantly elevated. Following treatment, it decreased and the CD4 + CXCR3 + CCR4- cell population increased. B) Neopterin and CXCL10 (IP-10) concentrations in CSF. Before treatment, both neopterin and CXCL10 (IP-10) concentrations were significantly elevated. Following treatment, both biomarkers decreased to within the range of the therapeutic goal for HAM patients.

cell population (Figure 4A), which conflicted with CNS relapse of ATL but was consistent with HAM (Natsumi et al. 2014). Furthermore, both the neopterin and CXCL10 (IP-10) concentrations in the CSF were significantly elevated (Figure 4B), although lower than those associated with aggressive HAM (14). Notably, the case was insufficient to fulfill the diagnostic criteria for HAM (Mitsuhiro 1990) because HTLV-I antibody (PA method) was negative in CSF.

Bacterial, fungal, and tuberculous encephalomyelopathies were excluded because no increase in cell numbers and no decline in glucose concentration in CSF were observed. Real-time polymerase chain reaction (PCR) testing for CMV, EBV, HSV, VZV, HHV-6, and JC virus in CSF showed negative results.

Serum soluble interleukin-2 receptor (sIL-2R) level was slightly elevated (Table 2), but significantly lower compared with that at the onset of ATL.

Not all of the results necessarily corresponded to CNS relapse of ATL, although we could not exclude it. We treated her with mPSL pulse and intrathecal injection of MTX + Ara-C + PSL. After one course of mPSL pulse, her crural paresis improved dramatically to such a degree that she could pull up to standing after a few days. Although she was given intrathecal injections four times weekly, her crural paresis was gradually exacerbated and progressed to paralysis. mPSL pulse was performed again, but the effect was limited.

We examined her CSF again but there was no increase in cells, and ATL cells could not be detected by microscopic examination. Furthermore, the MRI findings improved over time (Figure 2C), although her neurological findings worsened and HTLV-I proviral DNA could not be detected repeatedly in peripheral mononuclear cells (PBMCs) after allo-PBSCT. No evidence of relapsed ATL could be found and we continued 5 mg/day PSL thereafter while she continued rehabilitation.

The results of CSF analysis in May 2013 showed the following improvements. In flow cytometric analysis, the CD4 + CXCR3 + CCR4+ cell population had decreased and the normal CD4 + CXCR3 + CCR4- cell population had increased. Both neopterin and CXCL10 (IP-10) had decreased to within the range of the therapeutic goal for HAM patients (Figure 4A,B). Her paralysis improved gradually and steadily only by rehabilitation, to such a degree that she could walk when holding onto parallel bars.

Discussion

ATL with CNS involvement may occur during systemic progression of the disease and its frequency is estimated to be 10–25% (Kitajima et al. 2002). However, cases of CNS relapse without peripheral blood and lymph nodes of ATL have been reported (Marshall et al. 1998; Dungenwalla et al. 2005). In flow cytometric analysis of CSF of ATL patients, the CD4 + CXCR3-CCR4+ cell population is elevated. However, in the current case, the CSF fluid analysis revealed expansion of the CD4 + CXCR3 + CCR4+ cell population, which is consistent with HAM (Natsumi et al. 2014). Sato T et al. (Sato et al. 2013) reported increased neopterin and CXCL10 (IP-10) in HAM patients, and they were valuable biomarkers for disease progression of HAM. The neopterin and CXCL10 (IP-10) concentration in CSF paralleled the disease activity of HAM. The cut-off concentrations of neopterin and CXCL10 in HAM/TSP patients compared to HTLV-I infected non-HAM subjects are less than 5 pmol/mL and 200 pg/mL, respectively, and the CXCL10 (IP-10) concentration in the CSF of HAM patients with rapid progression is usually more than 5,000 pg/mL (Yamono, Y., personal communication). In the current case, we could not make a diagnosis of HAM because the CSF was negative for HTLV-I antibody in repeated examinations. Although the immunosuppressive status after allo-PBSCT might contribute, serum immunoglobulin levels

Table 2 Laboratory data on admission to our hospital in January 2013

WBC	4470/ μ l	GOT	15 IU/L	CRP	0.24 mg/dl
St	1.5%	GPT	33 IU/L	IgG	1390 mg/dl
Seg	64.0%	LDH	199 IU/L	IgA	51 mg/dl
Ly	14.0%	ALP	453 IU/L	IgM	352 mg/dl
Mo	19.5%	γ -GTP	87 IU/L		
Abnormal Ly	1.0%	TP	6.7 mg/dl	HTLV-I Ab	(+)
RBC	302×10^4 / μ l	Alb	3.5 mg/dl	HBs-Ag	(-)
Hb	9.5 g/dl	BUN	9.8 mg/dl	HBs-Ab	(-)
Hct	29.4%	Cre	0.56 mg/dl	HBc-Ab	(-)
MCV	97.4 fl	Na	133 mEq/L	HCV-Ab	(-)
MCH	31.5 pg	K	4.0 mEq/L	HIV-Ab	(-)
MCHC	32.3%	Cl	96 mEq/L		
Plt	12.0×10^4 / μ l	Corrected Ca	10.5 mg/dl		

were almost within normal limit at the same time period (Table 2) and there is not enough evidence to indicate false negative. In any inflammatory diseases of CNS, CXCR3+ cells but not CCR4+ cells were generally found in CSF (Misu et al. 2001). However, CXCR3 + CCR4+ double positive cells existed in her CSF. It was unlikely that CXCR3 + CCR4+ double positive cells emerged into CSF in nonspecific inflammatory condition. Given her background, we supposed these CCR4+ cells were HTLV-I infected cells, but the number of these cells was insufficient to measure HTLV-I viral load.

In the current case, neither CSF data nor clinical course consisted with CNS relapse of ATL. In case of ATL patients, CXCR3-CCR4+ T cell lymphocytes population expanded. Therapeutic effect was obtained from mPSL pulse rather than intrathecal injection. Furthermore, disease progression in the typical case of CNS relapse of ATL was more aggressive. We concluded some inflammatory condition caused by these HTLV-I infected cells may have developed HAM-like myelopathy.

CNS GVHD remains a controversial entity and it is difficult to establish an unequivocal diagnosis. Yet a few cases have been reported, who were suspected of CNS GVHD from brain biopsy or autopsy, their CSF showed predominant T-lymphocyte infiltration of donor origin (Kamble et al. 2007). In the current case, brain or spinal cord biopsy was not performed, and chimerism analysis of T cells in CSF was difficult because of the full-match HLA and sex-matched PBSCT. The number of T cells in CSF was insufficient to analyze chimerism using the short tandem repeat (STR) method. Neopterin (Niederwieser et al. 1984; Hempel et al. 1997) and CXCL10 (IP-10) (Mapara et al. 2006) levels in serum increase significantly in patients with active GVHD, but the levels in CSF are unknown. The possibility of active CNS GVHD could not be completely excluded. Both CXCR3 and CCR4 expression of T cells infiltrated in the CNS in patients with active CNS GVHD is unknown. It was no wonder that CXCR3+ cells in CSF were found in nonspecific inflammatory condition such as CNS GVHD, but unlikely that CCR4+ cells were.

The patient's neurological dysfunction seemed to fluctuate in parallel with the serum concentration of soluble interleukin-2 (sIL-2R) receptor (Figure 3). However, increased sIL-2R occurs not only with ATL relapse but also with HAM (Matsumoto et al. 1990), GVHD (Kami et al. 2000), and inflammatory neurogenic disorders caused by immunologic T-cell responses (Maier et al. 2009). Thus, it is difficult to make a definite diagnosis based on elevated sIL-2R alone.

In conclusion, we report a case with myelopathy without ATL relapse in the CNS. Flow cytometric analysis is helpful to differentiate immune-mediated encephalopathy or myelopathy from CNS relapse of ATL. If we encountered the patients suspected of CNS relapse of ATL, we should

consider the possibility of inflammatory condition caused by HTLV-I infected cells. Further analysis of pathology are warranted.

Competing interests

The authors declare that they have no competing interests.

Authors' contribution

TK participated in treatment for the patient and drafting the manuscript. NO, KS, MK, NJ and KY participated in treatment for the patient. YY carried out flow cytometric analysis and measurement of neopterin and CXCL10 (IP-10) concentration in CSF, and helped to draft the manuscript. RT participated in acquiring the data and helping to draft the manuscript. AT and KU supervised and helped to draft the manuscript. All authors read and approved the final manuscript.

Author details

¹Department of Hematology/Oncology, Research Hospital, The Institute of Medical Science, the University of Tokyo, 4-6-1 Shirokanedai, Minato-ku, Tokyo 108-8639, Japan. ²Division of Molecular Therapy, Department of The advanced Clinical Research Center, The Institute of Medical Science, the University of Tokyo, 4-6-1 Shirokanedai, Minato-ku, Tokyo 108-8639, Japan. ³Department of Blood Transfusion and Cellular Therapy, National Cancer Center Hospital, 5-1-1 Tsukiji, Chuo-ku, Tokyo 104-0045, Japan. ⁴Department of Rare Diseases Research, Institute of Medical Science, St. Marianna University Graduate School of Medicine, Sugao, Miyamae-ku, Kawasaki, Kanagawa 216-8512, Japan.

Received: 15 August 2014 Accepted: 22 September 2014

Published: 4 October 2014

References

- de Oliveira MF, Vieira M, Primo J, Siqueira IC, Carvalho EM, Farre L, Fatal PL, Bittencourt AL (2010) Flower cells in patients with infective dermatitis associated with HTLV-1. *J Clin Virol* 48:288–290
- Dungerwalla M, Osuji N, Waldman AD, Jehani FAI, Mehta A, Taylor R, Wotherspoon A, Cogill G, Matutes E (2005) Isolated central nervous system involvement in adult T-cell lymphoma/leukaemia. *Br J Haematol* 130:511–515
- Hempel L, Köhrholz D, Nussbaum P, Bönig H, Burdach S, Zintl F (1997) High interleukin-10 serum levels are associated with fatal outcome in patients after bone marrow transplantation. *Bone Marrow Transplant* 20:365–368
- Hinuma Y, Nagata K, Hanaoka M, Nakai M, Matsumoto T, Kinoshita K, Shirakawa S, Miyoshi I (1981) Adult T-cell leukemia: antigen in an ATL cell line and detection of antibodies to the antigen in human sera. *Proc Natl Acad Sci U S A* 78:6476–6480
- Kamble RT, Chang CC, Sanchez S, Carrum G (2007) Central nervous system graft-versus-host disease: report of two cases and literature review. *Bone Marrow Transplant* 39:49–52
- Kami M, Matsumura T, Tanaka Y, Mikami Y, Miyakoshi S, Ueyama J, Morinaga S, Mori S, Machida U, Kanda Y, Chiba S, Sakamaki H, Hirai H, Muto Y (2000) Serum levels of soluble interleukin-2 receptor after bone marrow transplantation: a true marker of acute graft-versus-host disease. *Leuk Lymphoma* 38:533–540
- Kami M, Hamaki T, Miyakoshi S, Murashige N, Kanda Y, Tanosaki R, Takaue Y, Taniguchi S, Hirai H, Ozawa K, Kasai M (2003) Allogeneic haematopoietic stem cell transplantation for the treatment of adult T-cell leukaemia/lymphoma. *Br J Haematol* 120:304–309
- Kitajima M, Korogi Y, Shigematsu Y, Murashige M, Kanda Y, Tanosaki R, Takaue Y, Taniguchi S, Hirai H, Ozawa K, Kasai M (2002) Central nervous system lesions in adult T-cell leukaemia: MRI and pathology. *Neuroradiology* 44:559–567
- Maier LM, Anderson DE, Severson CA, Baecher-Allan C, Healy B, Liu DV, Wittrup KD, De Jager PL, Hafler D (2009) Soluble IL-2RA levels in multiple sclerosis subjects and the effect of soluble IL-2RA on immune responses. *J Immunol* 182:1541–1547
- Mapara MY, Leng C, Kim YM, Bronson R, Loksbin A, Luster A, Sykes M (2006) Expression of chemokines in GVHD target organs is influenced by conditioning and genetic factors and amplified by GVHR. *Biol Blood Marrow Transplant* 12:623–634
- Marshall AG, Pawson R, Thom M, Shuz TF, Scaravilli F, Rudge P (1998) HTLV-I associated primary CNS T-cell lymphoma. *J Neurol Sci* 158:226–231
- Matsumoto M, Sugimoto M, Nakashima H, Imamura F, Kawano O, Uyama E, Takatsu K, Araki S (1990) Spontaneous T cell proliferation and release of